JCTC Journal of Chemical Theory and Computation

pubs.acs.org/JCTC Article

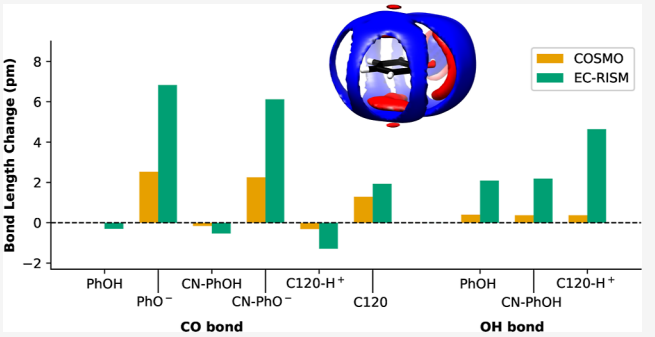
Implementation of EC-RISM for ADC(2) and CC2 to Include Solvent Granularity Effects in Excited-State Energies and Gradients

Julia Haberhauer,* Patrick Kibies, Stefan M. Kast, and Christof Hättig

Cite This: *J. Chem. Theory Comput.* 2026, 22, 6742−6760 Read Online

ACCESS | Metrics & More | Article Recommendations | Supporting Information

ABSTRACT: The embedded cluster reference interaction site model (EC-RISM) employs statistical-mechanical integral equation theory to predict solvent site distributions and their interaction with a solute using quantum-mechanical electronic structure methods. In contrast to apparent surface charge models such as the polarizable continuum (PCM) or the conductor-like screening (COSMO) model, EC-RISM can account for directional solvent−solute interactions due to the description of the solvent based on conventional molecular force field models. Here we present an implementation of EC-RISM combined with correlated wave function methods for ground- and excited-state energies and, for the first time, also for ground- and excited-state energy gradients. This is achieved by self-consistent equilibrating the solvent reaction field with the solute charge density in the correlated and, possibly, electronically excited state. To account for excitonic coupling and nonequilibrium contributions to electronic transition energies, EC-RISM is further combined with COSMO. We present applications to the molecular structures and the absorption and emission energies of 4-(*N*,*N*-dimethylamino)benzonitrile (DMABN), the photobase 7-amino-4-methylcoumarin, and the photoacids phenol and 3-cyanophenol in aqueous solution. As expected, for systems without strong directional solvent interactions, such as DMABN, EC-RISM yields results similar to those obtained with COSMO whereas, for molecules or ions that form strong hydrogen bonds to the solvent (particularly the deprotonated photoacids) EC-RISM provides substantial improvements.



1. INTRODUCTION

When modeling electronically excited states and electronic spectra of molecular systems in solution, their interaction with the solvent cannot be ignored. Solvent effects play a decisive role, as they can influence the electronic character of both the ground and the excited states of the solute, alter the relative positions or even the order of different states, and change their potential energy surfaces (PESs). This is particularly true for charge-transfer transitions, i.e., transitions between states with substantially different charge distributions. They can be shifted in solution by several tenths of an electronvolt depending on the solvent polarity. Other important examples are $n\pi^*$ transitions, which are often blue-shifted in solution. When the n orbital is a Brønsted basic site, this effect can in protic solvents also amount to several tenths of an electronvolt.

A fully quantum mechanical description of solute and solvent is computationally very demanding for electronic spectra and impractical for many electronic structure methods because of the large system size and the extensive sampling over solvent configurations that is required when the solvent is included explicitly. Mixed quantum mechanical/molecular mechanical (QM/MM) approaches, in which the solvent is described by a force field, provide an alternative that reduces the computational costs, but still require the sampling of hundreds of solvent configurations to obtain converged results.

A computational efficient approach to account for solvent effects in electronic structure calculations is provided by apparent surface charge (ASC) models originating from a dielectric continuum background as, e.g., the polarizable continuum model[1,2] (PCM) or the conductor-like screening model[3] (COSMO). These approaches employ macroscopic properties, such as the dielectric constant of the solvent, to model the interaction of the solute with a structureless distribution of the solvent. The advantages of such implicit solvent models are reduced computational costs and simplified computational protocols since no sampling over solvent configurations is needed, and widespread integration in quantum-chemical packages. A disadvantage of ASC models is that they do not account for the molecular structure of the solvent and therefore cannot describe explicit directional solute−solvent interactions, such as hydrogen bonding.

Received: March 5, 2026
Revised: May 13, 2026
Accepted: June 2, 2026
Published: June 15, 2026



ACS Publications

© 2026 The Authors. Published by American Chemical Society

Downloaded from pubs.acs.org/jctce/article-pdf/22/13/6742/6590849/acs.jctc.6c00419.pdf by RUHR UNIVERSITAET BOCHUM user on 21 August 2026

The embedded cluster reference interaction site model[4,5] (EC-RISM) employs an approach that is intermediate between continuum models and QM/MM. Similar to QM/MM approaches, it accounts for the molecular structure of the solvent; in contrast to the latter, however, it embeds the solute in a thermally averaged solvent site distribution that is determined using statistical-mechanical integral equation theory in the form of the three-dimensional reference interaction site model (3D-RISM),[6−8] using established force field models of the solvent species. The resulting spatially resolved solute−solvent interaction potential that accounts for the solvent's internal structure is particularly important for protic solvents and solutes with functional groups capable of forming hydrogen bonds. Since the solvent distribution preaverages over solvent configurations approximately compatible with the equilibrium ensemble, the electronic structure calculations for the solute do not need to be repeated for snapshots of a representative ensemble of solvent structures. Compared with the QM/MM approach, this implicit averaging reduces computational costs substantially, though not to a level comparable to that of continuum solvation models but with the added benefit of a more realistic description of a solvent environment.

One-dimensional (1D) and three-dimensional (3D) RISM variants have during the past decade been combined with electronic structure methods using various coupling schemes between electronic and liquid structure to compute energies and spectroscopic properties in solution.[9−17] While most applications used mean-field methods and were concerned with ground-state properties, for excitation energies only a few applications have been reported in refs 18−20 in combination with time-dependent density functional theory (TD-DFT). For an overview of the family of these so-called RISM-SCF (self-consistent field) methods to which EC-RISM belongs with its particular coupling scheme outlined in detail below, we refer to a recent review by Imamura et al.[21]

When a quantum system is embedded in a polarizable environment equilibrated with the charge distribution of the former, we are in the realm of self-consistent reaction field (SCRF) theory.[22] The density-dependent environment or reaction field potential introduces a nonlinearity into the Schrödinger equation that is not present for isolated quantum systems. Structurally, the density-dependence of the reaction field potential is very similar to that of the Coulomb potential in Hartree−Fock (HF) and density functional theory (DFT). For mean field methods it can readily be determined together with the Coulomb and exchange potentials by the self-consistent field (SCF) algorithm that is used to solve, e.g., the HF or Kohn−Sham equations. For post-SCF approaches like coupled cluster (CC) methods or algebraic diagrammatic construction (ADC) schemes, a fully self-consistent solution of the SCRF problem requires to iterate over the ground-state SCF and the post-SCF calculation until the electron density of the solute and the reaction field potential are equilibrated with each other. This scheme to couple the determination of the reaction field potential to the electronic structure calculation is in the literature often referred to as perturbation through the energy and density (PTED).[23] As approximations to PTED, the perturbation through the energy (PTE) and the perturbation through the density (PTD) approaches have been developed.[23]

For excited states, the nonlinear Schrödinger equation in SCRF theory leads in addition to the problem that—in contrast to the vacuum case—a specific self-consistent solution for each state yields different results than a linear-response (LR) calculation starting from the ground or some other initial state. The relaxation of the solvent's reaction field potential to the solute's new charge distribution after an electronic transition is only captured by the state-specific (SS) approach, while the excitonic coupling between the solute's transition density and the (electronic) response of the environment is only included by the linear-response approach.[24,25]

One possibility to account for this problem is the corrected linear response (cLR) model[26] where the excited-state free energies obtained from a LR calculation are corrected through first order by evaluating the polarization energy in the excited state with the excited-state densities obtained from a TDDFT calculation in vacuum.[26] Alternatives proposed within the framework of time-dependent density functional theory (TDDFT) are the self-consistent approach due to Improta, Barone, Scalmani, and Frisch (IBSF),[27] and the vertical excitation model (VEM) proposed by Marenich et al. in ref 28. For response theory based on correlated post-SCF wave function methods, Lunkenheimer and Köhn[25] proposed a generalization of the self-consistent PTED coupling scheme that includes both the LR and SS contributions, and presented an implementation for excitation energies at the COSMO-ADC(2) level. The latter reaction field coupling scheme, in the following denoted as PTED(LR), has recently been used to implement excited-state gradients in solution for ADC(2) and the approximate coupled cluster singles and doubles model[29] CC2 with a coupling scheme that accounts for LR and SS contributions.[30] In a previous publication,[31] we combined CC2 via the PTED scheme with EC-RISM to calculate vertical excitation energies for a set of photoacids and photobases in aqueous solution, neglecting LR and nonequilibrium corrections and using geometries optimized with COSMO-CC2 using a post-SCF coupling scheme.

In this work, MP2, ADC(2), and CC2 energies in ground and excited states are combined with EC-RISM as solvent model employing the PTED(LR) coupling scheme including linear response and nonequilibrium contributions. We present for the first time an implementation that includes analytic ground- and excited-state gradients for post-SCF electronic structure methods. The latter is facilitated by the self-consistent PTED and PTED(LR) coupling schemes and a representation of the solvent charge distribution and the solute's electrostatic potential on a joint 3D grid. Since EC-RISM describes the solvent on a fixed-charge force field level, the electronic solvent response alone can not be accounted for at this level. To account for effects arising solely from the electronic component, we implemented the option to include linear-response contributions and nonequilibrium corrections calculated with COSMO via a PTED(LR) coupling scheme.[31]

2. THEORETICAL BACKGROUND

2.1. The EC-RISM Solvent Model

Similar to DFT in electronic structure theory that describes the electronic energy as a functional of the electron density, the free energy of a fluid can be described as a functional of its particle densities. From the classical density functional theory (cDFT) formalism[32] the Ornstein−Zernike (OZ) equation can be derived, which relates different correlation functions in a fluid with each other.[33,34] The OZ equation was originally formulated for spherical particles but can be generalized to the

Downloaded from pubs.acs.org/jctce/article-pdf/22/13/6742/6590849/acs.jctc.6c00419.pdf by RUHR UNIVERSITAET BOCHUM user on 21 August 2026

https://doi.org/10.1021/acs.jctc.6c00419
J. Chem. Theory Comput. 2026, 22, 6742−6760

molecular Ornstein–Zernike (MOZ) equations for rigid anisotropic particles. The OZ equations are not complete, which is why so-called "closures" are needed to solve them; these are also derived from cDFT within suitable approximations. The solution of the MOZ equations is, however, computationally demanding, which led to the development of a hierarchy of RISM approximations that describe the full six-dimensional "direct" correlation functions (see below) of rigid bodies in a homogeneous liquid by superpositions of site–site (1D-RISM) or molecule-site (3D-RISM) correlation functions.

In 3D-RISM the total correlation function, $h(\mathbf{r})$, and a direct correlation function $c(\mathbf{r})$ between solute and solvent are connected via[7,8]

$$\rho_{\gamma,\infty} h_\gamma(\mathbf{r}) = \sum_{\gamma'} c_{\gamma'} \times \chi_{\gamma\gamma'}(\mathbf{r}') \tag{1}$$

Here, $\chi_{\gamma\gamma'}$ describes the solvent susceptibility (site–density correlation function, predetermined for a given solvent model typically from 1D-RISM calculations), ρ_γ the unperturbed bulk densities of the solvent sites and γ and γ' run over the solvent sites and "×" denotes a convolution operator. $h(\mathbf{r})$ is connected to the distribution function g via $h(\mathbf{r}) = g(\mathbf{r}) - 1$. For a solvable set of equations the above equation needs to be combined with a closure

$$h_\gamma(\mathbf{r}) = \exp(-\beta u_\gamma(\mathbf{r}) + h_\gamma(\mathbf{r}) - c_\gamma(\mathbf{r}) + B_\gamma(\mathbf{r})) - 1 \tag{2}$$

where u_γ is the interaction potential between the solute and the solvent site γ, $\beta = (k_B T)^{-1}$ and B is a bridge function[35] that formally accounts for approximations made during the derivation of the OZ equations and closure equations from cDFT as well as for the RISM superposition error. Omitting B leads to the hypernetted chain (HNC) closure[36,37]

$$h_\gamma(\mathbf{r}) = \exp(-\beta u_\gamma(\mathbf{r}) + h_\gamma(\mathbf{r}) - c_\gamma(\mathbf{r})) - 1 \tag{3}$$

The HNC closure can be approximated by a partial series expansion (PSE) through k-th order[4]

$$h_\gamma(\mathbf{r}) = \begin{cases} \exp(-\beta u_\gamma(\mathbf{r}) + h_\gamma(\mathbf{r}) - c_\gamma(\mathbf{r})) - 1 & \forall\ -\beta u(\mathbf{r}) - c_\gamma(\mathbf{r}) \le 0 \\ \sum_k \frac{1}{k!} (-\beta u_\gamma(\mathbf{r}) + h_\gamma(\mathbf{r}) - c_\gamma(\mathbf{r}))^k & \forall\ -\beta u(\mathbf{r}) - c_\gamma(\mathbf{r}) > 0 \end{cases} \tag{4}$$

where the first order (PSE-1) is equivalent to a closure proposed by Kovalenko and Hirata[38] (KH).

The excess chemical potential, μ^{ex}, which accounts for the contribution of the solute–solvent interaction and the changes in the solvent structure to the solvation free energy, is for the PSE closure in k-th order given by[35]

$$\mu^{ex}_{\text{PSE-}k} = \mu^{ex}_{\text{HNC}} - \frac{1}{\beta} \sum_\gamma \rho_\gamma \int \frac{(\Theta(h_\gamma(\mathbf{r}))(h_\gamma(\mathbf{r}) - \beta u_\gamma(\mathbf{r}) - c_\gamma(\mathbf{r}))^{k+1})}{(k+1)!}\, \mathrm{d}\mathbf{r} \tag{5}$$

where Θ is the Heaviside step function. The excess chemical potential for the HNC closure is[36,39]

$$\mu^{ex}_{\text{HNC}} = \frac{1}{\beta} \sum_\gamma \rho_\gamma \int \left(\frac{1}{2} h_\gamma^2(\mathbf{r}) - c_\gamma(\mathbf{r}) - \frac{1}{2} h_\gamma(\mathbf{r}) c_\gamma(\mathbf{r}) \right) \mathrm{d}\mathbf{r} \tag{6}$$

The interaction function, $u_\gamma(\mathbf{r})$, is composed of a Lennard-Jones and an electrostatic contribution, $u_\gamma = u_\gamma^{LJ} + u_\gamma^{ESP}$. The Lennard-Jones part is given by

$$u_\gamma^{LJ}(\mathbf{r}) = \sum_A 4\varepsilon_{A\gamma} \left[\left(\frac{\sigma_{A\gamma}}{|\mathbf{R}_A - \mathbf{r}|} \right)^{12} - \left(\frac{\sigma_{A\gamma}}{|\mathbf{R}_A - \mathbf{r}|} \right)^{6} \right] \tag{7}$$

where $\varepsilon_{A\gamma}$ and $\sigma_{A\gamma}$ are the mixed Lennard-Jones parameters for atom A of the solute and site γ of the solvent and $\mathbf{R}_A$ and $\mathbf{r}$ are the positions of, respectively, A and site γ. It depends only on the nuclear structure of the solute, but not on its electronic density. The electrostatic interaction is composed of a nuclear and an electronic contribution

$$\begin{aligned} u_\gamma^{ESP}(\mathbf{r}) &= q_\gamma \left[\sum_A \frac{Z_A}{|\mathbf{r} - \mathbf{R}_A|} + \int \frac{\rho_{sol}^{el}(\mathbf{r}')}{|\mathbf{r} - \mathbf{r}'|}\, \mathrm{d}\mathbf{r}' \right] \\ &= q_\gamma \int \frac{\rho_{sol}(\mathbf{r}')}{|\mathbf{r} - \mathbf{r}'|}\, \mathrm{d}\mathbf{r}' \end{aligned} \tag{8}$$

with the solute's nuclear charges Z_A, its (negative) electronic charge density ρ_{sol}^{el}, and the charge of the solvent site q_γ. With ρ_{sol} we denote the solute's total, i.e. nuclear plus electronic, charge density. In force field-based 3D-RISM calculations, electrostatic solute–solvent interactions are typically approximated by atomic site charges. For simplicity we use the conventional notation of the LJ potential and the electrostatic potential in atomic units (a.u.). Formally, unit-wise equivalence is achieved when the LJ parameters ε and σ are provided in a.u.

Besides the conceptual separation of solute–solvent interactions into LJ and electrostatic components discussed above, within 3D-RISM the total interaction is formally split into long-range and short-range parts, where the former is modeled by Ewald summation[40] over auxiliary atom-centered point charges. The difference between the exact electrostatic and the Ewald potential is added to the short-range potential,[41] compensating for the remaining small inconsistency between the periodic Ewald potential and the aperiodic, wave function-derived residual short-range potential by a switching scheme.[5,42]

To couple 3D-RISM with electronic structure calculations, we employ the embedded cluster RISM (EC-RISM) method.[4,5] In this approach, the solute, described by an electronic structure model, and the solvent, described by 3D-RISM, mutually polarize each other. The free energy of the solvated molecular system is defined as the sum of the internal energy of the solute, E_{sol}, and the excess chemical potential as $G = E_{sol} + \mu^{ex}$. For approximate electronic structure methods E_{sol} as well as the electronic charge density ρ_{sol}^{el} depend on some variable wave function parameters λ_k. For variational methods, like for instance HF or DFT, they are in vacuum determined by minimizing the energy. For nonvariational methods, like MP2, ADC(2), or CC2, the equations determining these parameters can be combined with the energy expression to a Lagrange function L_{sol} which is then required to be stationary with respect to variations of the λ_k. This is carried over to EC-RISM by replacing the vacuum expression for the energy by the free energy of the solvated system, i.e. for variational methods it is required that

Downloaded from pubs.acs.org/jctce/article-pdf/22/13/6742/6590849/acs.jctc.6c00419.pdf by RUHR UNIVERSITAET BOCHUM user on 21 August 2026

https://doi.org/10.1021/acs.jctc.6c00419
J. Chem. Theory Comput. 2026, 22, 6742–6760

$$\frac{\mathrm{d}G}{\mathrm{d}\lambda_k} = \frac{\mathrm{d}E_{\mathrm{sol}}}{\mathrm{d}\lambda_k} + \frac{\mathrm{d}\mu^{\mathrm{ex}}}{\mathrm{d}\lambda_k} = 0 \tag{9}$$

and for nonvariational methods that

$$\frac{\mathrm{d}G}{\mathrm{d}\lambda_k} = \frac{\mathrm{d}L_{\mathrm{sol}}}{\mathrm{d}\lambda_k} + \frac{\mathrm{d}\mu^{\mathrm{ex}}}{\mathrm{d}\lambda_k} = 0 \tag{10}$$

Additionally, stationarity of the excess chemical potential w.r.t. variations in the correlation functions is required, which follows from the variational principle derived for HNC and PSE closures.[35] The implicit dependence of the correlation functions on the wave function parameters λ_k leads to a coupling between the two variational conditions. In the variation of the free energy (or the respective Lagrangian) the optimizable parameters λ_k of the electronic wave function or density enter μ^{ex} only through the electronic density. Thus

$$\frac{\mathrm{d}\mu^{\mathrm{ex}}}{\mathrm{d}\lambda_k} = \int \frac{\delta\mu^{\mathrm{ex}}}{\delta\rho^{\mathrm{el}}_{\mathrm{sol}}(\mathbf{r}')} \frac{\mathrm{d}\rho^{\mathrm{el}}_{\mathrm{sol}}(\mathbf{r}')}{\mathrm{d}\lambda_k} \,\mathrm{d}\mathbf{r}' \tag{11}$$

where $\delta\mu^{\mathrm{ex}}$ depends on the interaction function. For the HNC and PSE closures, which include also the KH closure, Kast and Kloss and Kovalenko and Hirata showed that the variation of the excess chemical potential can be expressed in closed form as[35,38]

$$\delta\mu^{\mathrm{ex}} = \sum_\gamma \int \rho_\gamma(\mathbf{r}')\delta u_\gamma(\mathbf{r}') \,\mathrm{d}\mathbf{r}' = \sum_\gamma \rho_\gamma \int g_\gamma(\mathbf{r}')\delta u_\gamma(\mathbf{r}') \,\mathrm{d}\mathbf{r}' \tag{12}$$

using $\rho_\gamma(\mathbf{r}') = \rho_\gamma g_\gamma(\mathbf{r}')$. This formulation allows us, using eq 8, to write the functional derivative of μ^{ex} with respect to the solute charge density $\rho_{\mathrm{sol}}(\mathbf{r})$ as

$$\frac{\delta\mu^{\mathrm{ex}}}{\delta\rho_{\mathrm{sol}}(\mathbf{r})} = \sum_\gamma q_\gamma \int \frac{g_\gamma(r')}{|\mathbf{r} - \mathbf{r}'|} \,\mathrm{d}\mathbf{r}' \tag{13}$$

The derivative of the charge density with respect to the wave function parameters λ_k can be expressed as

$$\frac{\mathrm{d}\rho_{\mathrm{sol}}(\mathbf{r})}{\mathrm{d}\lambda_k} = \frac{\mathrm{d}\rho^{\mathrm{el}}_{\mathrm{sol}}(\mathbf{r})}{\mathrm{d}\lambda_k} = -\sum_{\mu\nu} \frac{\mathrm{d}D^{\mathrm{ao}}_{\mu\nu}}{\mathrm{d}\lambda_k} \chi^*_\mu(\mathbf{r})\chi_\nu(\mathbf{r}) \tag{14}$$

where D^{ao} is the density matrix in the basis of the atomic orbital (AO) χ_μ. Combining these results, the total derivative of μ^{ex} with respect to the wave function parameters λ_k can be written as

$$\frac{\mathrm{d}\mu^{\mathrm{ex}}}{\mathrm{d}\lambda_k} = -\sum_\gamma q_\gamma \iint \frac{g_\gamma(\mathbf{r}')}{|\mathbf{r} - \mathbf{r}'|} \sum_{\mu\nu} \frac{\mathrm{d}D^{\mathrm{ao}}_{\mu\nu}}{\mathrm{d}\lambda_k} \chi^*_\mu(\mathbf{r})\chi_\nu(\mathbf{r}) \,\mathrm{d}\mathbf{r}' \,\mathrm{d}\mathbf{r} \tag{15}$$

In the practical implementation, $\rho_\gamma(\mathbf{r})$ is discretized on a three-dimensional grid with points $\mathbf{r}_s$, each associated with a volume element D_s.

The grid points are arranged on a rectangular grid oriented along the coordinate axis with n_i points spaced by a distance d_i along the i-th axis. The grid is centered around the geometric center of the solute

$$\mathbf{R}_0 = \frac{1}{N_{\mathrm{at}}} \sum_A \mathbf{R}_A \tag{16}$$

Thus, the coordinates of the grid points $\mathbf{r}_s$ with compound indices $s = (s_x, s_y, s_z)$ are given by

$$r_{s,i} = R_{0,i} + d_i\left(s_i - \frac{n_i - 1}{2}\right) \qquad \text{with} \quad s_i = 1, \ldots, n_i \tag{17}$$

The solvent charge distribution is mapped onto point charges Q_s at these grid points $\mathbf{r}_s$ as

$$Q_s = \sum_\gamma q_\gamma \int_{D_s} g_\gamma(\mathbf{r}') \,\mathrm{d}\mathbf{r}' \tag{18}$$

where D_s is the volume element assigned to the grid point r_s. Consequently, the derivative expression becomes

$$\begin{aligned}\frac{\mathrm{d}\mu^{\mathrm{ex}}}{\mathrm{d}\lambda_k} &= -\sum_{\mu\nu} \frac{\mathrm{d}D^{\mathrm{ao}}_{\mu\nu}}{\mathrm{d}\lambda_k} \int \sum_s \chi^*_\mu(\mathbf{r}) \frac{Q_s}{|\mathbf{r}_s - \mathbf{r}|} \chi_\nu(\mathbf{r}) \,\mathrm{d}\mathbf{r} \\ &= \sum_{\mu\nu} \frac{\mathrm{d}D^{\mathrm{ao}}_{\mu\nu}}{\mathrm{d}\lambda_k} \sum_s Q_s V_{\mu\nu,s}\end{aligned} \tag{19}$$

with

$$V_{\mu\nu,s} = -\int \chi^*_\mu(\mathbf{r}) \frac{1}{|\mathbf{r}_s - \mathbf{r}|} \chi_\nu(\mathbf{r}) \,\mathrm{d}\mathbf{r} \tag{20}$$

For the following, we write the derivative of the excess chemical potential in short as derivative of the expectation value of an operator $\hat{G}^{\mathrm{env}}$ for the potential of the environment (i.e., the solvent)

$$\frac{\mathrm{d}\mu^{\mathrm{ex}}}{\mathrm{d}\lambda_k} = \frac{\mathrm{d}\langle\hat{G}^{\mathrm{env}}\rangle}{\mathrm{d}\lambda_k} \tag{21}$$

with

$$\hat{G}^{\mathrm{env}} = \sum_s Q_s \hat{V}_s \tag{22}$$

We note that $\hat{G}^{\mathrm{env}}$ depends through the charges Q_s on the density matrix. In the following we will sometimes make this explicit by writing $\hat{G}^{\mathrm{env}}(\mathbf{D})$. In the context of self-consistent reaction field theory[22] $\hat{G}^{\mathrm{env}}$ is also referred to as reaction field (potential) operator. In the molecular orbital (MO) basis, $\hat{G}^{\mathrm{env}}$ can be expressed in second quantization as

$$\hat{V}_s = -\sum_{pq} \left\langle p \left| \frac{1}{|\mathbf{r}_s - \mathbf{r}|} \right| q \right\rangle \hat{E}_{pq} \tag{23}$$

where p and q denote general MOs and $\hat{E}_{pq}$ are the second quantization singlet excitation operators.[43]

For EC-RISM-Hartree–Fock, the intensive, i.e. per-particle free energy is given by the sum of the solute's internal energy obtained as expectation value of $\hat{H}^{\mathrm{QM}}$ and the chemical excess potential

$$G_{\text{EC-RISM-HF}} = \langle \mathrm{HF}|\hat{H}^{\mathrm{QM}}|\mathrm{HF}\rangle + \mu^{\mathrm{ex}}(\mathbf{D}^{\mathrm{HF}}) \tag{24}$$

with the density matrix $\mathbf{D}^{\mathrm{HF}}$. The HF determinant can be parametrized as

$$|\mathrm{HF}\rangle = \exp\Big(\sum_{\mu_0} \kappa_{\mu_0}(E_{\mu_0} - E^\dagger_{\mu_0})\Big)|\mathrm{HF}_0\rangle \tag{25}$$

with orbital rotation parameters κ_{μ_0} and a reference determinant HF_0. The indices μ_0 run over all orbital pairs $p < q$ for which the Fock matrix elements are requested to vanish

Downloaded from pubs.acs.org/jctce/article-pdf/22/13/6742/6590849/acs.jctc.6c00419.pdf by RUHR UNIVERSITAET BOCHUM user on 21 August 2026

https://doi.org/10.1021/acs.jctc.6c00419
J. Chem. Theory Comput. 2026, 22, 6742−6760

(vide infra), at least all occupied/virtual pairs. Minimizing the free energy w.r.t. the κ_{μ_0} leads for EC-RISM-HF to the Brillouin condition

$$0 = \langle \mathrm{HF}|[\hat{H}^{\mathrm{QM}} + \hat{G}^{\mathrm{env}}, E_{\mu_0} - E^{\dagger}_{\mu_0}]|\mathrm{HF}\rangle \tag{26}$$

It can be fulfilled, e.g., by solving the nonlinear eigenvalue problem for an embedded Fock operator $\hat{F}^{\mathrm{emb}}$ consisting of a vacuum-like part $\hat{F}^{\mathrm{QM}}$ and the above-defined (see eq 22) reaction field operator

$$\hat{F}^{\mathrm{emb}}|\mathrm{HF}\rangle = (\hat{F}^{\mathrm{QM}}(\mathbf{D}^{\mathrm{HF}}) + \hat{G}^{\mathrm{env}}(\mathbf{D}^{\mathrm{HF}}))|\mathrm{HF}\rangle = \sum_{i=1}^{n_{\mathrm{el}}} \epsilon_i|\mathrm{HF}\rangle \tag{27}$$

These equations can be solved by the usual self-consistent field algorithms. The only difference for EC-RISM-HF compared to the vacuum case is that now in each iteration in addition to $\hat{F}^{\mathrm{QM}}$ also $\hat{G}^{\mathrm{env}}$ has to be evaluated, after the electrostatic potential has been determined on the grid points $\mathbf{r}_s$ and the 3D-RISM equations have been solved. The same approach can be used for Kohn−Sham DFT.

As pointed out in the introduction, the fully self-consistent minimization becomes somewhat more involved for post-SCF methods where the equations for additional electronic parameters have to be considered. As discussed for COSMO in refs 25 and 30, a fully variational minimization which facilitates the evaluation of analytic gradients w.r.t. the nuclear coordinates, can be derived when the solvent is equilibrated with the orbital-relaxed charge density for the respective electronic structure method.

2.2. Orbital-Relaxed One-Electron Densities for MP2, ADC(2) and CC2

To introduce the notation for the post-HF methods CC2, MP2, and ADC(2) and the theoretical background for the orbital-relaxed one-electron densities, we start with the approximate coupled cluster singles and doubles model[29] CC2. This model is an approximation to CCSD which gives ground-state energies and excitation energies for single excitations that are correct through second order in the electron fluctuation potential $\hat{W} = \hat{H} - \hat{F}$. As for other CC methods, the CC2 energy is obtained as[29]

$$E_{\mathrm{CC2}} = \langle \mathrm{HF}|\hat{H}\exp(\hat{T})|\mathrm{HF}\rangle \tag{28}$$

The cluster operator $\hat{T}$ consists for CC2 of a sum of a single excitation part, $\hat{T}_1$, and a double excitation part, $\hat{T}_2$, which can be written as

$$\hat{T}_1 = \sum_{\mu_1} t_{\mu_1}\hat{\tau}_{\mu_1} \tag{29}$$

$$\hat{T}_2 = \sum_{\mu_2} t_{\mu_2}\hat{\tau}_{\mu_2} \tag{30}$$

The amplitudes t_{μ_1} and t_{μ_2} are determined by the cluster equations

$$0 = \langle \mu_1|\widehat{\hat{H}} + [\widehat{\hat{H}}, \hat{T}_2]|\mathrm{HF}\rangle \tag{31}$$

$$0 = \langle \mu_2|\widehat{\hat{W}} + [\hat{F}, \hat{T}_2]|\mathrm{HF}\rangle \tag{32}$$

Above, we used $\hat{T}_1$-similarity transformed operators $\widehat{\hat{O}} = \exp(-\hat{T}_1)\hat{O}\exp(\hat{T}_1)$. With $\langle\mu_1|$ and $\langle\mu_2|$ we denote the singly and doubly excited bra states.[43]

The expression for the CC energy, 28, the cluster equations, 31 and 32, and the Brillouin condition, $0 = \langle \mathrm{HF}|[\hat{H}, \hat{E}_{\mu_0} - \hat{E}^{\dagger}_{\mu_0}]|\mathrm{HF}\rangle$, are combined to a Lagrange function

$$\begin{aligned} L_{\mathrm{CC2}}(\overline{t}, t, \overline{\kappa}, \kappa) &= \langle \mathrm{HF}|\widehat{\hat{H}} + [W, \hat{T}_2]|\mathrm{HF}\rangle + \langle \mathrm{HF}|[\hat{H}, \kappa]|\mathrm{HF}\rangle \\ &+ \langle \overline{t}_1|H + [W, \hat{T}_2]|\mathrm{HF}\rangle + \langle \overline{t}_2|W + [\hat{F}, \hat{T}_2]|\mathrm{HF}\rangle \end{aligned} \tag{33}$$

with $\langle \overline{t}_i| = \sum_{\mu_i} \overline{t}_{\mu_i}\langle \mu_i|$ for $i = 1, 2$ and $\widehat{\overline{\kappa}} = \sum_{\mu_0} \overline{\kappa}_{\mu_0}(\hat{E}_{\mu_0} - \hat{E}^{\dagger}_{\mu_0})$. The variables $\overline{t}_{\mu_1}$, $\overline{t}_{\mu_2}$, and $\overline{\kappa}_{\mu_0}$ are Lagrange multipliers for, respectively, the cluster amplitude equations and the Brillouin condition, and are determined by requiring L_{CC2} to be stationary in t_{μ_1}, t_{μ_2}, and κ_{μ_0}.

From the variational Lagrange function for the CC2 ground-state energy, the elements of the orbital-relaxed one-electron ground-state density matrix are obtained as the coefficients for the integrals for the one-electron part of $\hat{H}$[44]

$$\begin{aligned} D^{\mathrm{CC2,eff}}_{pq} &= \langle \mathrm{HF}|\exp(-\hat{T}_1)\hat{E}_{pq}\exp(\hat{T}_1) + [\hat{E}_{pq}, \widehat{\overline{\kappa}}]|\mathrm{HF}\rangle \\ &+ \langle \overline{t}_1|\exp(-\hat{T}_1)([\hat{E}_{pq}, \hat{T}_2] + \hat{E}_{pq})\exp(\hat{T}_1)|\mathrm{HF}\rangle \\ &+ \langle \overline{t}_2|[\hat{E}_{pq}, \hat{T}_2]|\mathrm{HF}\rangle \end{aligned} \tag{34}$$

The excitation energies are obtained in CC response theory as the eigenvalues of the Jacobian for the residual of the cluster equations, 31 and 32. For CC2, the Jacobian has the form[29]

$$\mathbf{A}^{\mathrm{CC2}} = \left(\begin{array}{c|c} \langle \mu_1|[\widehat{\hat{H}} + [\hat{H}, \hat{T}_2], \hat{\tau}_{\nu_1}]|\mathrm{HF}\rangle & \langle \mu_1|[\widehat{\hat{H}}, \hat{\tau}_{\nu_2}]|\mathrm{HF}\rangle \\ \hline \langle \mu_2|[\widehat{\hat{H}}, \hat{\tau}_{\nu_1}]|\mathrm{HF}\rangle & \langle \mu_1|[\hat{F}, \hat{\tau}_{\nu_2}]|\mathrm{HF}\rangle \end{array}\right) \tag{35}$$

We note that $\mathbf{A}^{\mathrm{CC2}}$ is non-Hermitian and has, thus, different right, E^f, and left, $\overline{E}^f$, eigenvectors. The total energy of an excited state f is determined as the sum of the respective excitation energies ω^f and the CC2 ground-state energy. Hence, the Lagrange function for the excited state consists of the sum of the Lagrange function for the ground state, the excitation energies expressed through the Jacobian and the eigenvectors, and the condition for the biorthonormality of the eigenvectors[45]

$$\begin{aligned} L^f_{\mathrm{CC2}}(\overline{t}^f, t, \overline{\kappa}^f, \kappa, E^f, E^f, \omega^f) &= L_{\mathrm{CC2}}(\overline{t}^f, t, \overline{\kappa}^f, \kappa) \\ &+ \sum_{i,j=1}^{2}\sum_{\mu_i\nu_j} \overline{E}^f_{\mu_i} A^{\mathrm{CC2}}_{\mu_i\nu_j} E^f_{\nu_j} + \omega^f\Big(1 - \sum_{i=1}^{2}\sum_{\mu_j} \overline{E}^f_{\mu_i} E^f_{\mu_j}\Big) \end{aligned} \tag{36}$$

In the above equation, the upper index f indicates that the Lagrange multipliers $\overline{t}^f$ and $\overline{\kappa}^f$, the excitation energy ω^f, and the right and left eigenvectors E^f and $\overline{E}^f$ depend on the selected excited state. The orbital-relaxed one-electron density matrix in the excited state is, thus, obtained as[45]

https://doi.org/10.1021/acs.jctc.6c00419
J. Chem. Theory Comput. 2026, 22, 6742−6760

Downloaded from pubs.acs.org/jctce/article-pdf/22/13/6742/6590849/acs.jctc.6c00419.pdf by RUHR UNIVERSITAET BOCHUM user on 21 August 2026

$$D_{pq}^{\mathrm{CC2},f,\mathrm{eff}} = \langle \mathrm{HF}|\exp(-\hat{T}_1)\hat{E}_{pq}\exp(\hat{T}_1) + [\hat{E}_{pq}, \hat{\bar{\kappa}}^f]|\mathrm{HF}\rangle + \langle \bar{t}_1^f|\exp(-\hat{T}_1)([\hat{E}_{pq}, \hat{T}_2] + \hat{E}_{pq})\exp(\hat{T}_1)|\mathrm{HF}\rangle + \langle \bar{t}_2^f|[\hat{E}_{pq}, \hat{T}_2]|\mathrm{HF}\rangle + \langle \bar{E}_1^f|\exp(-\hat{T}_1)[\hat{E}_{pq}, \hat{E}_1^f + \hat{E}_2^f]\exp(\hat{T}_1)|\mathrm{HF}\rangle + \langle \bar{E}_2^f|[\hat{E}_{pq}, \hat{E}_2^f]|\mathrm{HF}\rangle \quad (37)$$

with $\hat{E}_i^f = \sum_{\mu_i}\hat{E}_{\mu_i}^f\hat{\tau}_{\mu_i}$ and $\langle\bar{E}_i| = \sum_{\mu_i}\bar{E}_{\mu_i}\langle\mu_i|$.

An alternative to CC theory to include electron correlation effects is Møller−Plesset perturbation theory (MPPT). In its second order, i.e. in MP2, it provides an energy which is in accuracy comparable to that of CC2, but with simplified amplitude equations that can be solved noniteratively. In particular, in its spin-unrestricted form or for closed-shell cases it includes only contributions from double excitations, $\hat{T}_2$, and the equations for the amplitudes and the MP2 energy can be derived from eqs 32 and 28 by discarding the contributions from $\hat{T}_1$. The respective Lagrangian can be expressed as

$$L_{\mathrm{MP2}}(\bar{t}, t, \bar{\kappa}, \kappa) = \langle \mathrm{HF}|\hat{H} + [\hat{W}, \hat{T}_2]|\mathrm{HF}\rangle + \langle \bar{t}_2|\hat{W} + [\hat{F}, \hat{T}_2]|\mathrm{HF}\rangle + \langle \mathrm{HF}|[\hat{H}, \hat{\bar{\kappa}}]|\mathrm{HF}\rangle \quad (38)$$

and the corresponding orbital-relaxed one-electron density matrix becomes

$$D_{pq}^{\mathrm{MP2,eff}} = \langle \mathrm{HF}|\hat{E}_{pq} + [\hat{E}_{pq}, \hat{\bar{\kappa}}]|\mathrm{HF}\rangle + \langle \bar{t}_2|[\hat{E}_{pq}, \hat{T}_2]|\mathrm{HF}\rangle \quad (39)$$

We note that for MP2 the Lagrange multipliers $\bar{t}_{\mu_2}$ are the adjoints of the amplitudes so that no additional equation needs to be solved for them.

For describing excited states with MP2 as corresponding ground state model, the ADC(2) method is suitable. In ADC(2), excitation energies are obtained as eigenvalues of a secular matrix[46,47] which has some similarities to the CC2 Jacobian,[48] but is, in contrast to the latter, HermitianAbove

$$\mathbf{A}^{\mathrm{ADC(2)}} = \left(\begin{array}{c|c} \frac{1}{2}\hat{P}_{\mu_1,\nu_1}\langle\mu_1|[\hat{H} + [\hat{H}, \hat{T}_2], \hat{\tau}_{\nu_1}]|\mathrm{HF}\rangle & \langle\mu_1|[\hat{H}, \hat{\tau}_{\nu_2}]|\mathrm{HF}\rangle \\ \hline \langle\mu_2|[\hat{H}, \hat{\tau}_{\nu_1}]|\mathrm{HF}\rangle & \langle\mu_2|[\hat{F}, \hat{\tau}_{\nu_2}]|\mathrm{HF}\rangle \end{array}\right) \quad (40)$$

$\hat{P}_{\mu_1,\nu_1}$ is a symmetrization operator defined by $\hat{P}_{\mu_1,\nu_1}f(\mu_1, \nu_1) = f(\mu_1, \nu_1) + f(\nu_1, \mu_1)$. ADC(2) uses for $\hat{T}_2$ the first-order double excitation amplitudes from MPPT from which also the MP2 energy is obtained. Accordingly, the Lagrangian for the excited-state energy defined as the sum of the MP2 ground-state energy and ADC(2) excitation energy for state f is obtained as

$$L_{\mathrm{ADC(2)}}^f(\bar{t}^f, t, \bar{\kappa}^f, \kappa, E^f, \bar{\omega}^f) = L_{\mathrm{MP2}}(\bar{t}^f, t, \bar{\kappa}^f, \kappa) + \sum_{i,j=1}^{2}\sum_{\mu_i\nu_j}\bar{E}_{\mu_i}^f A_{\mu_i\nu_j}^{\mathrm{ADC(2)}}E_{\nu_j}^f + \omega^f\left(1 - \sum_{i=1}^{2}\sum_{\mu_i}\bar{E}_{\mu_i}^f E_{\mu_i}^f\right) \quad (41)$$

The orbital-relaxed one-electron density becomes

$$D_{pq}^{\mathrm{ADC(2)},f,\mathrm{eff}} = \langle \mathrm{HF}|\hat{E}_{pq} + [\hat{E}_{pq}, \hat{\bar{\kappa}}^f]|\mathrm{HF}\rangle + \langle \bar{t}_2^f|[\hat{E}_{pq}, \hat{T}_2]|\mathrm{HF}\rangle + \langle \bar{E}_1^f|[\hat{E}_{pq}, \hat{E}_1^f + \hat{E}_2^f]|\mathrm{HF}\rangle + \langle \bar{E}_2^f|[\hat{E}_{pq}, \hat{E}_2^f]|\mathrm{HF}\rangle \quad (42)$$

We used above still $\bar{E}^f$ and E^f for the eigenvectors, but note that for ADC(2) they are the adjoints of each other and, thus, only the eigenvalue equation for one of them needs to be solved.

2.3. The PTED Coupling Scheme

As mentioned in the Introduction, for post-SCF methods different reaction field coupling schemes have been discussed in the literature to account for the mutual polarization of the solute and the solvent. For ground-state energies with correlated wave function methods like CC and MPPT, these are in particular the PTE and the PTED schemes.[23] For the current work, we focus on PTED which iterates over the equations that determine the (charge) distributions of the solvent and the electron density of the solute until the energy and the density are self-consistent and, thus, the free energy or the respective Lagrange function have become stationary. The PTED-ADC(2) approach was first implemented by Lunkenheimer and Köhn[25] in combination with COSMO for excitation energies. Recently, Hättig and Pausch[30] generalized the implementation to cover in addition PTED-CC2 ground-state and excitation energies, and nuclear gradients for PTED-MP2, PTED-ADC(2) and PTED-CC2.

When the solvent is equilibrated with the orbital-relaxed electron density, no additional boundary conditions and thus Lagrange multipliers are needed compared to the vacuum case and the free energy Lagrangian is simply the sum of the vacuum-like Lagrangian and the excess chemical potential. For example for PTED-EC-RISM-MP2 we obtain as Lagrangian

$$L_{\text{PTED-MP2}}(\bar{t}, t, \bar{\kappa}, \kappa) = L_{\mathrm{MP2}}(\bar{t}, t, \bar{\kappa}, \kappa) + \mu^{\mathrm{ex}}(\mathbf{D}^{\mathrm{MP2,eff}}) \quad (43)$$

The changes in the equations for the electronic parameters, i.e. orbital rotation parameters, cluster amplitudes, Lagrange multipliers, and eigenvectors are small: Compared to the vacuum case, the Fock operator has to be replaced by $\hat{F}^{\mathrm{emb}} = \hat{F}^{\mathrm{QM}} + \hat{G}^{\mathrm{env}}(\mathbf{D})$ and the iterations and the convergence check for the self-consistent equilibration of the solute and the solvent have to be added. The PTED scheme is implemented in TURBOMOLE[49,50] with the `ricc2` program[51] as follows:

1. The HF equations are solved in the first iteration either for the vacuum case or self-consistently for EC-RISM-HF, in all other iterations for a fixed reaction-field evaluated from predetermined solvent charges (vide infra).
2. The post-HF calculation for the correlated ground-state energy or excitation energy is done. This includes the solution of the cluster equations, and, for excited states, the solution of the eigenvalue problem.
3. This is followed by the solution of the equations for the Lagrange multipliers and the determination of the orbital-relaxed one-electron density matrix for the correlated ground or excited state.
4. The electrostatic potential of the solute is evaluated on the grid and the 3D-RISM equations are solved.

Downloaded from pubs.acs.org/jctce/article-pdf/22/13/6742/6590849/acs.jctc.6c00419.pdf by RUHR UNIVERSITAET BOCHUM user on 21 August 2026

https://doi.org/10.1021/acs.jctc.6c00419
J. Chem. Theory Comput. 2026, 22, 6742−6760

Thereafter, the excess chemical potential and the solvent charges Q_s are calculated.

5. If the changes in the free energy and the root-mean-square and maximal changes in the solvent charges are below preset convergence thresholds, the procedure is terminated, else it continues with step 1.

After convergence, the self-consistently determined orbital-relaxed one-electron density can be used to calculate one-electron properties that are derivatives of the free energy Lagrangians w.r.t. the weights of the corresponding operators in the Hamiltonian.

2.4. Analytic Gradients for the Solute within EC-RISM

The variational nature of the PTED approach facilitates in particular the calculation of nuclear gradients for the free energy. Due to the stationarity of the Lagrangian, eq 10, or, for Hartree−Fock, the free energy, eq 9, the total derivatives of G become the partial derivatives with respect to the nuclear coordinates X_A

$$\frac{\mathrm{d}G}{\mathrm{d}X_A} = \frac{\partial L_{\mathrm{sol}}}{\mathrm{d}X_A} + \frac{\partial \mu^{\mathrm{ex}}}{\mathrm{d}X_A} \tag{44}$$

where for Hartree−Fock $L_{\mathrm{sol}} = E_{\mathrm{sol}}$. The expressions for derivatives of the vacuum-like part $\partial L_{\mathrm{sol}}/\mathrm{d}X_A$ for ADC(2) and CC2 have been reported e.g. in refs 44, 45, and 48 The 3D-RISM contribution to the gradient consists of contributions from the Lennard-Jones and the electrostatic interaction potentials[52]

$$\frac{\partial \mu^{\mathrm{ex}}}{\partial X_A} = \sum_\gamma \rho_\gamma \int g_\gamma \left(\frac{\mathrm{d}u_\gamma^{\mathrm{LJ}}(\mathbf{r})}{\mathrm{d}X_A} + \frac{\mathrm{d}u_\gamma^{\mathrm{ESP}}(\mathbf{r})}{\mathrm{d}X_A} \right) \mathrm{d}\mathbf{r} \tag{45}$$

Before proceeding with the derivation of the gradient with respect to the nuclear coordinates, it is important to consider translational invariance. As pointed out above, the grid is kept centered around the geometric center of the solute, $\mathbf{R}_0$, eq 16. In the gradient calculation, this needs to be taken into account by including the contributions from the partial derivatives with respect to the grid point positions x_s. The electrostatic part, related to the second term in eq 45, is given by

$$\frac{\partial \mu^{\mathrm{ex,ESP}}}{\partial X_A} = \sum_s Q_s \frac{\mathrm{d}V_s}{\mathrm{d}X_A} - \sum_{\alpha\beta} F_{\alpha\beta}^{\mathrm{eff,pol}} S_{\alpha\beta}^{[X_A]} \tag{46}$$

with

$$\frac{\mathrm{d}V_s}{\mathrm{d}X_A} = \frac{\partial V_{A,s}}{\partial X_A} - \sum_{\alpha\beta} D_{\alpha\beta}^{\mathrm{ao}} V_{\alpha\beta,s}^{[X_A]} + \frac{1}{N_{\mathrm{at}}} \frac{\partial V_s}{\partial x_s} \tag{47}$$

$$F_{\alpha\beta}^{\mathrm{eff,pol}} = \frac{1}{2} \sum_{pq} C_{\alpha p} C_{\beta q} \sum_r \left(D_{pr} G_{rq}^{\mathrm{env}}(\mathbf{D}) + D_{rq} G_{pr}^{\mathrm{env}}(\mathbf{D}) \right) \tag{48}$$

The derivatives of the electrostatic potentials at the grid points V_s consist of a nuclear contribution arising from $V_{A,s} = \frac{Z_A}{|X_s - X_A|}$, an electronic contribution containing the derivatives of the AO integrals for the electrostatic potentials $V_{\alpha\beta,s}^{[X_A]}$ contracted with the density matrix in the AO basis, $\mathbf{D}^{\mathrm{ao}}$, and the contribution from the derivatives w.r.t. to the grid point positions where x_s is the component of r_s along the same axis as X_A. The latter contribution arises from keeping the grid centered in the geometric center of the solute. $\mathbf{S}^{[X_A]}$ are the derivatives of the overlap integrals in the AO basis and $C_{\alpha p}$ the MO coefficients. (For further details, we refer to the Supporting Information). Similarly the LJ part is given by

$$\frac{\mathrm{d}\mu^{\mathrm{ex,LJ}}}{\mathrm{d}X_A} = \sum_\gamma \rho_\gamma \int g_\gamma(\mathbf{r}) \left[\frac{\partial u_\gamma^{\mathrm{LJ}}(\mathbf{r})}{\partial X_A} + \frac{1}{N_{\mathrm{at}}} \sum_s \frac{\partial u_\gamma^{\mathrm{LJ}}(\mathbf{r})}{\partial x_s} \right] \mathrm{d}\mathbf{r} \tag{49}$$

The vacuum-like contributions and the contributions from the electrostatic interaction potential are evaluated for HF and DFT in the `grad` and `rdgrad` programs and for MP2, ADC(2), and CC2 in the `ricc2` program of the TURBOMOLE package.[49,50] Provided the box for the 3D integration grid is large enough, the above treatment of the electrostatic interaction in the electronic structure calculation is consistent with that for the solution of the RISM equations without and with long-range correction[5,42] for the electrostatic potential. The LJ part[52] is evaluated in the `rism` program[4,5,12,42,53] and added to the latter contributions.

2.5. Effects from the Fast Solvents Response on Electronic Transitions

The PTED scheme equilibrates the solvent with the charge density of a given state which then enters through the reaction field potential $\hat{G}^{\mathrm{env}}$ in the Schrödinger equation. When considering electronic excitations, it has on the one hand the advantage that it fully accounts for the reorganization of the solvent following an excitation, including both the nuclear and the electronic relaxation of the solvent. On the other hand it has the disadvantage that it does not account for the excitonic coupling between the solute's transition density and the dynamic (electronic) charge density susceptibility of the solvent[25,54,55] which appears naturally in linear response theory applied to a reference state obtained from a self-consistent reaction field calculation. A physically meaningful modeling of the excitonic coupling or LR contribution requires, however, a description of the dynamic electronic response of the solvent.

The different time scales for the electronic (fast) and nuclear (slow) response of the solvent also affects electronic transition frequencies in the solute: while the initial state has often lived long enough to assume that the solvent's electronic as well as nuclear degrees of freedom are in equilibrium with the solute's charge density in this state, only the fast electronic degrees of freedom can follow electronic transitions instantaneously. This can be modeled approximately by adding nonequilibrium corrections (vide infra) to the transition energies obtained with a reaction field potential frozen in the initial state.

Since EC-RISM does not distinguish between nuclear and electronic contributions due to the fixed-charge force field model of the solvent species, we can use it only to model the total nuclear plus electronic response of the solvent. To account for the effects that arise only from the electronic component, we implemented the possibility to include linear response contributions and nonequilibrium corrections calculated with COSMO while the total response is described with EC-RISM. The difference between COSMO calculations with and without LR contributions was already used in refs 20 and 31 to correct excitation energies computed with EC-RISM as solvent model. Here, we integrate these contributions in calculations that use otherwise EC-RISM to evaluate the reaction field from the total (nuclear plus electronic) response of the solvent. This has the advantage that the LR and nonequilibrium corrections are evaluated with the total and

Downloaded from pubs.acs.org/jctce/article-pdf/22/13/6742/6590849/acs.jctc.6c00419.pdf by RUHR UNIVERSITAET BOCHUM user on 21 August 2026

https://doi.org/10.1021/acs.jctc.6c00419
J. Chem. Theory Comput. 2026, 22, 6742−6760

transition density matrices from the EC-RISM calculation. It avoids ambiguities in cases where configuration mixing between excited states is sensitive to the solvent model and allows to include the LR contribution in gradient calculations.

2.5.1. COSMO. In the conductor-like screening model, the solvent is approximated as a homogeneous dielectric continuum. The solute is enclosed within a molecular-shaped cavity, and the interaction between the solute and solvent is represented by charges distributed on the cavity surface. The latter are calculated for the fast electronic contribution as[3,25]

$$Q_s^{\text{fast}}(\mathbf{D}) = -f(n^2)\sum_t [\mathcal{A}^{-1}]_{st} V_t(\mathbf{D}) \tag{50}$$

where $\mathcal{A}$ is the response kernel for COSMO,[3] $V_t(\mathbf{D})$ the electrostatic potential due to the solute's charge density at a surface site t, and $f(n^2)$ a scaling factor that depends on the refractive index of the solvent[3,25]

$$f(n^2) = \frac{n^2 - 1}{n^2 + 0.5} \tag{51}$$

With these surface charges the reaction field $\hat{G}^{\text{fast}}$ is calculated as

$$\hat{G}^{\text{fast}}(\mathbf{D}) = \sum_s Q_s^{\text{fast}}(\mathbf{D})\hat{V}_s \tag{52}$$

where $\hat{V}_s$ is defined as in eq 23, but now for a site on the cavity surface.

2.5.2. Linear Response. In the COSMO variant of the algebraic diagrammatic construction linear-response contributions appear up to second order only in the singles/singles block of the secular matrix[25]

$$\mathbf{A}^{\text{ADC(2),LR}}_{\mu_1,\nu_1} = \frac{1}{2}\hat{P}_{\mu_1,\nu_1}\sum_s \langle \mu_1|\hat{V}_s + [\hat{V}_s, \hat{T}_2]|\text{HF}\rangle \langle \text{HF}|[\hat{Q}_s^{\text{fast}}, \hat{\tau}_{\nu_1}]|\text{HF}\rangle \tag{53}$$

For CC2 they are similar but less symmetric[30]

$$\mathbf{A}^{\text{CC2,LR}}_{\mu_1,\nu_1} = \sum_s \langle \mu_1|\widehat{\widehat{V}}_s + [\widehat{\widehat{V}}_s, \hat{T}_2]|\text{HF}\rangle\langle \text{HF}|[\hat{Q}_s^{\text{fast}}, \hat{\tau}_{\nu_1}]|\text{HF}\rangle \tag{54}$$

The operators $\hat{Q}_s^{\text{fast}}$ are defined analogously to Q_s^{fast}, but with V_t replaced by $\hat{V}_t$. As previously stated, upon convergence of the SCRF iterations, the free energy Lagrangian becomes stationary. This remains valid when linear response (LR) contributions are included, which facilitates the implementation of nuclear gradients. To express them in a compact form, we introduce two auxiliary transition densities[30] which are for CC2 defined as

$$D^{\xi,f}_{pq} = \langle \bar{E}_1^f|e^{-\hat{T}_1}(\hat{E}_{pq} + [\hat{E}_{pq}, \hat{T}_2])\, e^{\hat{T}_1}|\text{HF}\rangle \tag{55}$$

$$D^{\eta,f}_{pq} = \langle \text{HF}|[\hat{E}_{pq}, \hat{E}_1^f]|\text{HF}\rangle \tag{56}$$

For ADC(2) the expressions are formally the same, but with $\hat{T}_1 = 0$ and the left and right eigenvectors are adjoints of each other. With these densities, the nuclear derivative of the linear response contribution to the excited-state Lagrangian can be expressed for both methods as

$$\frac{\partial L^{\text{LR}}}{\partial X_A} = \sum_s Q_s^{\text{fast}}(\mathbf{D}^{\xi,f})\sum_{\alpha\beta} D^{\eta,f}_{\alpha\beta} V^{[X_A]}_{\alpha\beta,s} + \sum_s Q_s^{\text{fast}}(\mathbf{D}^{\eta,f})\sum_{\alpha\beta} D^{\xi,f}_{\alpha\beta} V^{[X_A]}_{\alpha\beta,s} - \sum_{\alpha\beta} F^{\text{eff,LR}}_{\alpha\beta} S^{[X_A]}_{\alpha\beta} - \frac{1}{f(n^2)}\sum_{st} Q_s^{\text{fast}}(\mathbf{D}^{\xi,f})\frac{\partial \mathcal{A}_{st}}{\partial X_A} Q_t^{\text{fast}}(\mathbf{D}^{\eta,f}) \tag{57}$$

where

$$F^{\text{eff,LR}}_{\alpha\beta} = \frac{1}{2}\sum_{pq} C_{\alpha p}C_{\beta q}\sum_r (D^{\xi,f}_{pr} G^{\text{fast}}_{rq}(\mathbf{D}^{\eta,f}) + D^{\xi,f}_{rq} G^{\text{fast}}_{pr}(\mathbf{D}^{\eta,f})) + \frac{1}{2}\sum_{pq} C_{\alpha p}C_{\beta q} \sum_r (D^{\eta,f}_{pr} G^{\text{fast}}_{rq}(\mathbf{D}^{\xi,f}) + D^{\eta,f}_{rq} G^{\text{fast}}_{pr}(\mathbf{D}^{\xi,f})). \tag{58}$$

2.5.3. Nonequilibrium State-Specific Correction. So far, we have considered the full reorganization of the solvent, including both nuclear and electronic relaxation (vide supra), i.e. equilibrium situations. We now look at electronic transitions in a solute that is initially in a state i with the solvent in equilibrium with the solute's charge distribution in this state. After a vertical electronic transition to a final state f only the fast (electronic) polarization is assumed to adapt to the change in the solute's electronic charge density, while the slow (nuclear) polarization remains in this initial state. The electrostatic contribution to the free energy in the final state is in this nonequilibrium situation given by

$$G^{f,\text{neq}}_{\text{elstat}} = \sum_s \left(Q_s^{i,\text{slow}} V_s(\mathbf{D}^f) + Q_s^{f,\text{fast}} V_s(\mathbf{D}^f) - \frac{1}{2} Q_s^{i,\text{slow}} V_s(\mathbf{D}^i) - \frac{1}{2} Q_s^{f,\text{fast}} V_s(\mathbf{D}^f) \right) \tag{59}$$

Here, the first two terms represent the electrostatic interaction energy between solute in the final state ($V_s(\mathbf{D}^f)$) and, respectively, the slow (nuclear) part of the solvent charges fixed in the initial state i and the fast electronic part of the solvent charges equilibrated with the final state f. The last two terms represent the work required to polarize the environment for both the slow and fast parts. In terms of the free energy of the solvated system in the initial state, $G^{i,\text{eq}}$, and the electronic excitation energy, $\Delta E_{f,i(\text{eq})}$, calculated for the solute with the fixed reaction field potential for the initial state, the free energy in the final state including the solute's internal energy is obtained as[25]

$$G^{f,\text{neq}} = L^{i,\text{eq}}_{\text{sol}} + \Delta E_{f,i(\text{eq})} + G^{i,\text{eq}}_{\text{elstat}} + \frac{1}{2}\sum_s (Q_s^{f,\text{fast}} - Q_s^{i,\text{fast}})(V_s(\mathbf{D}^f) - V_s(\mathbf{D}^i)) \tag{60}$$

For EC-RISM $G^{i,\text{eq}} = L^{i,\text{eq}}_{\text{sol}} + \mu^{\text{ex},i(\text{eq})}$ and includes in addition to the electrostatic interaction also the LJ interaction. (A detailed derivation is given in the Supporting Information.) The latter are assumed to remain upon vertical electronic transitions entirely in the initial state. The last term in eq 60 is a nonequilibrium correction to the free energy of the final state f after a vertical transition from the initial state i. For the combination of EC-RISM with COSMO, this correction term is evaluated with COSMO using the electron densities

https://doi.org/10.1021/acs.jctc.6c00419
J. Chem. Theory Comput. 2026, 22, 6742−6760

Downloaded from pubs.acs.org/jctce/article-pdf/22/13/6742/6590849/acs.jctc.6c00419.pdf by RUHR UNIVERSITAET BOCHUM user on 21 August 2026

obtained in the EC-RISM calculation with COSMO linear response contributions.

The work flow for PTED-EC-RISM calculations including the calculation of gradients and vertical transition energies with nonequilibrium corrections is shown Figure 1.

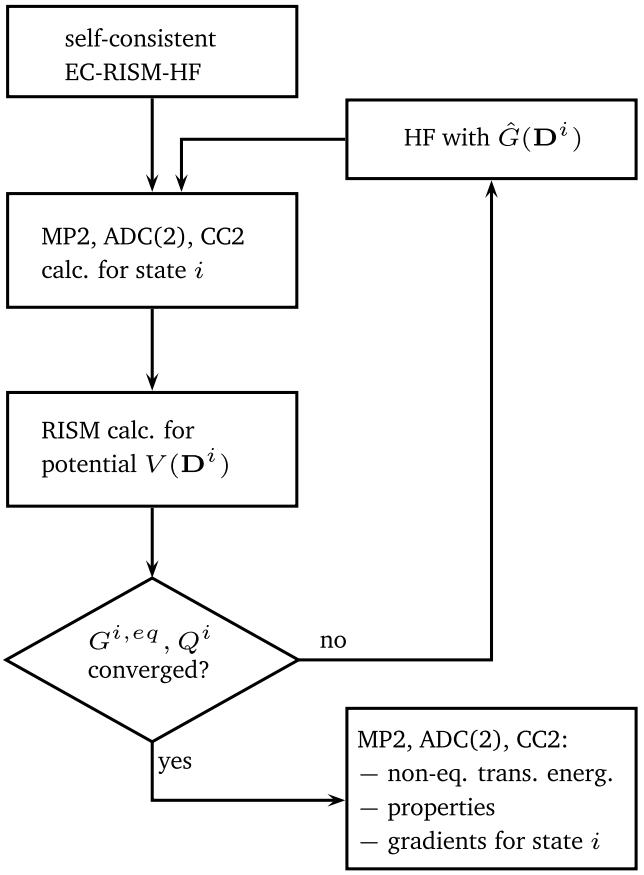


Figure 1. Flowchart for a PTED calculation including nonequilibrium transition energies for vertical excitation from the equilibrated state i to some final states or gradients for the equilibrated state i.

3. COMPUTATIONAL DETAILS

3.1. Electronic Structure Calculations

For all electronic structure calculations a development version of TURBOMOLE V7.9 has been used.[49,50] If not stated otherwise, geometries have been optimized for the ground and excited states with the def2-TZVPP basis[56] set. Refined excitation energies were then calculated at the optimized structures in the def2-TZVPPD basis[57] sets. Except for the test molecule 4-(*N*,*N*-dimethylamino)benzonitrile, abbreviated as DMABN, (see below), geometry optimizations were done at the MP2 level for the ground state and at the ADC(2) level for the excited state. DMABN has been used as an example for which the CC2 method has been applied. For all excited-state geometry optimizations, calculations with and without LR contributions were done and excitation energies were computed with and without LR and nonequilibrium contributions.

The Hartree−Fock calculations have been done with the dscf[58] program and CC2, MP2, and ADC(2) calculations with the ricc2 program.[48,51,59,60] The latter calculations employed the resolution-of-the-identity (RI) approximation for the electron repulsion integrals with auxiliary basis sets from refs 61, 62, optimized for the respective def2-TZVPP and def2-TZVPPD orbital basis sets. A SCF convergence criterion of 10^{-7} a.u. for the energy and 10^{-7} for the density were employed. All correlated calculations used the frozen core approximation for the $1s^2$ cores of all non-hydrogen atoms. For geometry optimization, convergence criteria of 10^{-4} a.u. were chosen for the maximum displacement and gradient, and 5×10^{-5} a.u. for the root-mean-square displacement and gradient.

3.2. EC-RISM and COSMO

All calculations with EC-RISM and COSMO were performed for aqueous solutions using the self-consistent PTED coupling scheme with convergence criteria of 10^{-6} a.u. for the energy and the maximum changes of the solvent charges. For COSMO, we used a dielectric constant ϵ = 78.447 and a refractive index of 1.33 and employed the Gaussian charge model with the default cavity parameters.[63] For EC-RISM, the solvent distribution was evaluated at T = 298.15 K and p = 1 bar with a solvent density of 0.033 329 50 Å^{-3}. A modified SPC/E water model[5] was used together with a dielectric constant of ϵ = 78.447 and the PSE-2 and PSE-3 closures. The Lennard-Jones parameters for the solute−solvent interaction were determined using Antechamber 22 with GAFF 1.81.[64] The 3D-RISM calculations were performed on a cubic grid with 128 lattice points per axis and a grid spacing of 0.3 Å. The convergence criterion for the 3D-RISM calculations was set to 10^{-6} for the maximum residual of the direct correlation functions. Geometry optimizations with EC-RISM have been carried out using the exact electrostatic potential. For the final single-point energies, the correction compensating for the small inconsistency between periodic and aperiodic potential described in refs 5 and 42 was applied. The auxiliary atom-centered point charges for the Ewald summation were calculated using the Merz−Kollman scheme with standard radii.[65,66]

4. RESULTS

In the following, we discuss the influence of the solvent model on optimized geometries (in ground and excited states) as well as on excitation and fluorescence energies. As representative examples, we consider the four molecules shown in Figure 2 and compare results obtained without a solvent model, with PTED-COSMO, and with PTED-EC-RISM using the PSE-2 and PSE-3 closures.

DMABN is a well-known system exhibiting dual fluorescence from both a locally excited and a charge transfer state. Phenol and 3-cyanophenol are photoacids, while 7-amino-4-methylcoumarin (also known as coumarin 120 or AMC) is a photobase.[67] Further information on the influence of the grid parameters for EC-RISM, basis set, natural transition orbitals

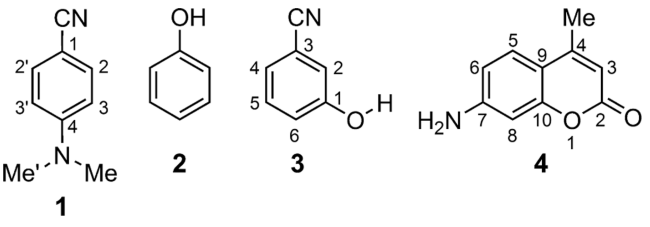


Figure 2. Structures studied in this work. For 3-cyanophenol, the NC0 conformer is shown, in which the hydroxy group points toward the cyano group. In the conformer NC1 it points toward C_6.

Downloaded from pubs.acs.org/jctce/article-pdf/22/13/6742/6590849/acs.jctc.6c00419.pdf by RUHR UNIVERSITAET BOCHUM user on 21 August 2026

https://doi.org/10.1021/acs.jctc.6c00419
J. Chem. Theory Comput. 2026, 22, 6742−6760

(NTOs), and timings can be found in the Supporting Information.

4.1. The TICT System 4-(Dimethylamino)benzonitrile

DMABN is a prototypical system exhibiting twisted intramolecular charge transfer (TICT). In the ground state, the phenyl ring and the dimethylamino group are coplanar whereas in the excited state they adopt a twisted configuration. Following electronic excitation to $S_2(L_a)$, the molecule first relaxes to a locally excited (LE) minimum on S_1. From this minimum, fluorescence can occur, or the system can, in polar solvents, relax to a TICT minimum. Consequently, depending on the polarity of the solvent, DMABN exhibits dual fluorescence resulting from both the LE minimum and the TICT minimum.

Experimentally, the twist in the S_1(TICT) state is evidenced by a large Stokes shift of approximately 9800 cm^{-1} in polar solvents such as 1-chlorobutane and by an almost forbidden emission.[69,70] In computational studies, both the electronic structure method and the treatment of solvent effects play significant roles. In vacuum, DMABN has, at the CC2/TZVPP level, a C_2-symmetric minimum for the LE state and a C_s-symmetric minimum for the TICT state, with the amino group tilted by $\phi = 41°$ out of the phenyl plane and rotated by $\tau = 90°$.[71] Close to the TICT minimum a C_{2v}-symmetric saddle point with a tilting angle of $\phi = 0°$ was found. PTED(LR)-COSMO geometry optimizations at the CC2/def2-TZVPP level[30] for acetonitrile as solvent yield a TICT minimum with $\phi = 0°$ and $\tau = 90°$. The LE state, however, is located in a flat region of the potential energy surface with a small but nonvanishing gradient toward the TICT mininum, causing the calculation to converge directly to the TICT minimum. This observation has been attributed to residual electron correlation errors of the second-order methods ADC(2) and CC2.

In the present work, we employed DMABN as a test case for solvent effects on structures and transition energies in a system where hydrogen-bonding effects are expected to be moderate. Therefore, qualitatively similar results with EC-RISM and COSMO are expected. The results for the ground-state structure of DMABN and the corresponding excitation energies are summarized in Table 1, while Table 2 summarizes the optimized geometries and emission energies for the TICT and the LE states. In aqueous solution, no minimum was found for the S_1(LE) state. For both COSMO and EC-RISM, the LE structure lies in a flat region of the potential energy surface, from which the optimization converges without a barrier to the TICT minimum. This is consistent with the results reported for other polar solvents using PTED(LR)-COSMO in ref 30 and reflects an underestimation of the TICT minimum energy by CC2. Consequently, the structure with the smallest residual gradient was chosen as representative for the LE state with EC-RISM and COSMO. Since no well-defined minimum was found for COSMO and EC-RISM, comparisons should be treated with caution (vide infra).

Table 1. DMABN, Ground State[a]

	vac	COSMO	PSE-2	PSE-3
ω (deg)[b]	24	18	14	14
$d(C_1C_2)$[c]	140.2	140.5	140.4	140.4
$d(C_2C_3)$[c]	138.7	138.6	138.3	138.3
$d(C_3C_4)$[c]	141.4	141.9	141.7	141.7
$d(C_4N)$[c]	137.8	136.5	135.9	135.9
$\Delta E(S_1(L_b))$	4.39	4.29	4.31	4.31
$\Delta E(S_1(L_b))$ LR[e]		4.27 (4.25)	4.28 (4.26)	4.28 (4.26)
$\Delta E(S_2(L_a))$[d]	4.70	4.45	4.44	4.43
$\Delta E(S_2(L_a))$ LR[d,e]		4.36 (4.34)	4.35 (4.32)	4.35 (4.32)

[a]Comparison of the most important geometric parameters and vertical excitation energies. Structures optimized with CC2/def2-TZVPP. Excitation energies with CC2/def2-TZVPPD. [b]Wagging angle of the amino group. Here defined as angle between the plane of C_{Me}, C'_{Me} and N and the line of N and C_4. [c]Bond distances in pm. [d]Experimental measurements yielded an L_a absorption band maximum of 4.17 eV.[68] [e]Nonequilibrium corrected energies given in parentheses.

For both the ground and TICT states, the equilibrium structures obtained with EC-RISM using the PSE-2 and PSE-3 closures agree within the numerical precision given in Tables 1 and 2. This indicates that solvent effects on the ground-state structure are small and that hydrogen-bonding effects are minor for the TICT state. The structures obtained with and without LR contributions also agree within the reported precision, consistent with the charge-transfer character of the transition and the correspondingly small transition density.

For the ground and the TICT state, also the geometries obtained with COSMO and EC-RISM are similar. In the ground state, the C_2C_3 and C_4N bond lengths and the wagging angle ω decrease from vacuum to COSMO to EC-RISM, indicating increasing conjugation of the amino lone pair with the π system. At the TICT minimum, the solution structures retain $\phi = 0°$ and $\tau = 90°$, whereas $\phi = 41°$ in vacuum. The largest TICT-state bond-length change relative to vacuum is the shortening of C_3C_4 by 3.0 pm with COSMO and 3.4 pm with EC-RISM.

For the approximate LE structures, the trends should be interpreted cautiously because no true minimum was located. The twist angle τ increases in solution with negligible dependence on the solvent model, whereas small nonzero values of ϕ and ω occur only with EC-RISM.

Compared to the gas phase, excitation to S_1 is red-shifted by up to 0.12 eV in solution, and absorption to S_2 by up to 0.35 eV. The choice of the solvent model has only a minor influence: the maximum difference between COSMO and EC-RISM is 0.02 eV, and the maximum difference between PSE-2 and PSE-3 0.01 eV. The LR contribution is −0.03 eV for S_1 and −0.09 eV for S_2, while the nonequilibrium correction is −0.03 eV. The experimentally measured L_a transition in water has its band maximum at 4.17 eV.[68] With LR and nonequilibrium contributions included, the COSMO and EC-RISM results for $\Delta E(S_2(L_a))$ deviate from the experimental by only 0.17 and 0.15 eV respectively. The remaining difference between the experimental and calculated excitation energy is most likely mostly due to the comparison of band maxima with vertical excitation energies.[72]

For emission from the TICT state, the excitations in solution are red-shifted relative to vacuum. The PSE order has a maximum influence of 0.01 eV, while the LR and nonequilibrium contributions amount to 0.07 and 0.19 eV, respectively. An emission energy of 2.38 eV has been measured for the TICT state.[68] As known from previous studies, higher-order correlation effects beyond CC2 are important for accurate transition energies at the deformed TICT structure of DMABN. CC2 underestimates vertical deexcitation energies as the TICT minimum[30] by ≳0.4 eV. The emission from the LE state was measured[68] as 3.25 eV, but due to the

Downloaded from pubs.acs.org/jctce/article-pdf/22/13/6742/6590849/acs.jctc.6c00419.pdf by RUHR UNIVERSITAET BOCHUM user on 21 August 2026

https://doi.org/10.1021/acs.jctc.6c00419
J. Chem. Theory Comput. 2026, 22, 6742−6760

Table 2. DMABN, LE and TICT States[a]

	vac	COSMO	COSMO-LR	PSE-2	PSE-2-LR	PSE-3	PSE-3-LR
				LE[b]			
τ (deg)[c]	19	44	24	24	23	not conv.	not conv.
$d(C_1C_2)$[d]	141.3	144.3	140.5	140.4	140.4		
$d(C_2C_3)$[d]	143.6	139.0	144.8	144.6	144.4		
$d(C_3C_4)$[d]	141.6	139.8	140.0	139.7	139.8		
$d(C_4N)$[d]	138.8	148.8	142.4	142.6	142.4		
$\Delta E(S_1)$[e,f]	3.76	2.54	3.17 (3.22)	3.06	2.85 (2.92)		
				TICT			
ϕ (deg)[g]	−41	0	0	0	0	0	0
$d(C_1C_2)$[d]	143.0	144.6	144.6	144.3	144.3	144.3	144.3
$d(C_2C_3)$[d]	137.3	137.8	137.8	137.7	137.7	137.7	137.7
$d(C_3C_4)$[d]	144.7	141.7	141.7	141.3	141.3	141.3	141.3
$d(C_4N)$[d]	144.3	143.1	143.1	142.8	142.8	142.8	142.8
$\Delta E(S_1)$[e,h]	2.48	1.63	1.63 (1.82)	1.60	1.53 (1.72)	1.59	1.52 (1.71)

[a]Comparison of the most important geometric parameters and vertical transition energies. Structures optimized with CC2/def2-TZVPP. Transition energies with CC2/def2-TZVPPD. [b]Norm of remaining gradients: COSMO 2×10^{-2} a.u., COSMO LR 4×10^{-4} a.u., PSE-2 3×10^{-3} a.u., PSE-2 LR 6×10^{-3} a.u. [c]Twist angle of the amino group. Here defined as average of the dihedrals $C_3C_4NC_{Me}$ and $C_3'C_4NC_{Me}'$. [d]Bond distances in pm. [e]Nonequilibrium corrected energies given in parentheses. [f]The experimental value for the LE emission band maximum is 3.25 eV.[68] [g]Out-of-plane angle of the amino group. Here defined as angle between the plane of C_3, C_3' and C_4 and the line of N and C_4. [h]The experimental value for the TICT emission band maximum is 2.38 eV.[68]

uncertainties in the CC2 LE structures, an accurate comparison with computed results is not possible.

4.2. Photoacids and Photobases

Photoacids are compounds that are more acidic in the excited state than in the ground state, where the relevant excited state is usually the state reached by the lowest singlet transition with significant oscillator strength. Photobases are correspondingly more basic in the electronically excited state. These properties make photoacids and photobases prime examples of solvent effects on excitation energies and are relevant for a variety of applications.[73] The smallest organic photoacids include phenol and phenol derivatives, whereas typical organic photobases include (amino-)quinolines or 7-amino-coumarine derivatives.

The thermodynamic principles behind photoacids and the Förster cycle, which is one possible thermodynamic cycle for quantifying the acidity change upon excitation, is shown in Figure 3. The Gibbs energy difference for the acid dissociation in the excited state, ΔG^*, can via the Förster cycle be expressed through the corresponding Gibbs energy difference in the ground state, ΔG, and the Gibbs energy changes upon excitation for the acid and its conjugated base, $\Delta G_{exc}(ROH)$ and $\Delta G_{exc}(RO^-)$, respectively. This leads for the change of the pK_a value upon excitation to the equation

$$\begin{aligned}\Delta pK_a^* &= pK_a^* - pK_a \\ &= \frac{\Delta G^* - \Delta G}{RT \ln 10} \\ &= \frac{\Delta G_{exc}(RO^-) - \Delta G_{exc}(ROH)}{RT \ln 10}\end{aligned} \quad (61)$$

where T is the temperature and R the molar gas constant. At standard temperature, T = 298.15 K, the inverse of the numerator becomes $1/(RT \ln 10) = 16.9044\ eV^{-1}$. In experimental studies that evaluate pK_a values via the Förster cycle, ΔG_{exc} is usually approximated by band maxima, whereas computational studies typically use vertical transitions.

The ability of the solvent to donate hydrogen bonds has a large effect on the excitation energies of aryl oxy anions, such as phenolate, which is not captured by continuum solvation models such as COSMO.[31] Hydrogen bonds to the solvent are also expected to influence the structure of photoacids and the conjugated bases, making them an important test case for structure optimizations with solvent models.

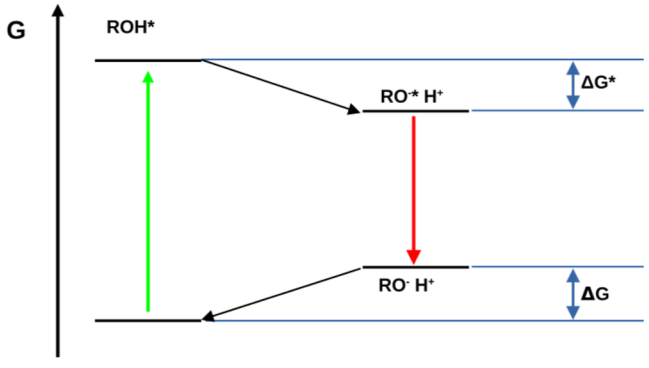


Figure 3. Förster cycle illustrating the thermodynamic principles of photoacidity. The equilibria between the acid/base pairs ROH/RO⁻ and ROH*/RO⁻* are related to each other by the transition energies for ROH/ROH* and RO⁻/RO⁻*.

4.2.1. Phenol. The results for the ground-state structures of phenol and the phenolate anion, as well as the corresponding excitation energies, are summarized in Table 3. Table 4 lists the optimized excited-state geometries and emission energies. Several trends can be observed:

- For the ground-state minimum of the deprotonated species, the CO bond length increases from vacuum to COSMO by 3.6 pm and further from COSMO to EC-RISM by 3.9−4.3 pm. For neutral phenol, the CO bond length changes only slightly with solvation, whereas the OH bond lengthens and the angle α increases slightly from vacuum to COSMO and further from COSMO to EC-RISM.
- In the excited state, the CO bond shortens for both the phenolate anion and neutral phenol as the solvent description becomes more physically appropriate. For neutral phenol, the OH bond length and α again

https://doi.org/10.1021/acs.jctc.6c00419
J. Chem. Theory Comput. 2026, 22, 6742−6760

Downloaded from pubs.acs.org/jctce/article-pdf/22/13/6742/6590384/acs.jctc.6c00419.pdf by RUHR UNIVERSITAET BOCHUM user on 21 August 2026

Table 3. Comparison of the Most Important Geometric Parameters and Vertical Excitation Energies of PhOH/PhO$^-$ for the Ground State[a]

	vac	COSMO	PSE-2	PSE-3
		PhO$^-$ Anion		
$d(C_1O)$[b]	126.9	129.5	133.4	133.8
$\Delta E(S_1)$[c]	3.23	4.12	4.71	4.75
$\Delta E(S_1)$ LR[c,d]		4.08 (4.05)	4.68 (4.66)	4.72 (4.71)
		PhOH		
$d(C_1O)$[b]	136.8	136.8	136.5	136.5
$d(OH)$[b]	96.2	96.5	97.8	98.3
$\alpha(C_1OH)$ (deg)	108	109	110	110
$\Delta E(S_1)$[e]	4.96	4.98	5.02	5.01
$\Delta E(S_1)$ LR[d,e]		4.95 (4.95)	5.00 (4.99)	4.99 (4.99)
		pK_a Change		
ΔpK_a^*	−29.17	−14.45	−5.24	−4.40
ΔpK_a^* LR[d]		−14.82 (−15.18)	−5.40 (−5.56)	−4.54 (−4.68)

[a]Optimized with MP2/def2-TZVPP. Excitation energies with ADC(2)/def2-TZVPPD. [b]Bond distances in pm. [c]For the anion the absorption band maximum was reported as 4.33 eV by Wehry and Rogers[74] and 4.21 eV by Joung et al.[75] [d]LR results include linear response contributions. Nonequilibrium corrected energies given in parentheses. [e]The experimentally measured absorption band maximum for the neutral species was reported by Wehry and Rogers[74] at 4.59 eV and by Joung et al.[75] at 4.54 eV.

increase from vacuum to COSMO and from COSMO to EC-RISM.

- The PSE order and LR contributions have only small structural effects, except for coordinates directly involved in hydrogen bonding. The largest LR-induced change is the shortening of the CO bond in phenolate, by up to 1.3 pm with EC-RISM and 0.7 pm with COSMO.
- A comparison of phenol in the ground and the excited state shows that upon excitation the CO bond shortens, while the OH bond lengthens and α increases. These effects become stronger from vacuum to COSMO and further to EC-RISM, with the CO bond showing the largest change.
- For the phenolate anion, the CO bond length increases by 9.9 pm in vacuum, but this effect is partially canceled by COSMO and almost completely canceled by EC-RISM through solvent induced charges in the CO bond length.

LR, nonequilibrium, and PSE-order effects are small for neutral phenol and moderate for phenolate, typically below 0.05 eV. The dominant effect is the change from COSMO to EC-RISM for the phenolate anion, where the absorption energy increases by 0.63−0.66 eV and the total solvent shift reaches 1.48 eV with PSE-3 including LR and nonequilibrium contributions. For neutral phenol, the difference between COSMO and EC-RISM is at most 0.05 eV.

The experimentally measured absorption band maximum for phenol in aqueous solution was reported as 4.59 eV by Wehry and Rogers[74] and as 4.54 eV by Joung et al.[75] The vertical excitation energies obtained with CC2 are blue-shifted by about 0.4 eV relative to those values, largely independent of the solvent description. About 0.1 eV of this deviation can be attributed to electron correlation contributions beyond CC2.[31] Most of the remaining deviation is most likely due to the difference between vertical transition energies and band maxima.[76] For the phenolate anion, the COSMO-CC2 absorption energies are red-shifted by ∼0.1−0.3 eV relative to the experimental band maximum reported as 4.33 eV (ref 74) and 4.21 eV (ref 75), whereas the EC-RISM-CC2 results are blue-shifted by up to 0.39 eV. Since higher-order correlation effects on the L_b excitation energy are small for phenolate,[31] most of the blue shift must be attributed to the comparison of vertical excitation energies with band maxima. In any case, band maximum are usually $\gtrsim$0.1 eV below the vertical transition. The red shift obtained with COSMO for the vertical transition energy of the phenolate anion indicates a significant error of the solvent model for this system which can be attributed to COSMO's inability to describe hydrogen bonds between solute and solvent. The agreement between calculated ΔpK_a^* values and the value of −4.30 determined from experimental band maxima is greatly improved when COSMO is replaced by EC-RISM.[31] The best agreement is obtained with PSE-3, which gives in combination with CC2 results between −4.40 and −4.68 depending on the inclusion of LR and nonequilibrium corrections.

For emission, the solvent-model dependence remains small for neutral phenol, with a maximum difference of 0.06 eV. PSE-order, nonequilibrium, and excitonic-coupling effects are likewise small for phenol and only slightly larger for phenolate, reaching at most 0.05−0.06 eV.

Table 4. Comparison of the Most Important Geometric Parameters and of the Vertical Transition Energies of PhOH/PhO$^-$ for the Excited State[a]

	vac	COSMO	COSMO-LR	PSE-2	PSE-2-LR	PSE-3	PSE-3-LR
				PhO$^-$ Anion			
$d(C_1O)$[b]	136.8	135.7	135.0	135.1	133.9	135.1	133.8
$\Delta E(S_1)$[c,d]	2.89	3.16	3.17 (3.23)	3.31	3.37 (3.42)	3.33	3.39 (3.44)
				PhOH			
$d(C_1O)$[b]	135.1	134.6	134.4	134.1	133.8	133.9	133.6
$d(OH)$[b]	96.7	97.2	97.2	98.9	98.9	99.8	99.9
$\alpha(C_1OH)$ (deg)	108	109	109	111	111	111	112
$\Delta E(S_1)$[c,e]	4.58	4.56	4.52 (4.52)	4.56	4.52 (4.52)	4.54	4.50 (4.51)
				pK_a Change[c]			
ΔpK_a^*	−28.60	−23.52	−22.81 (−22.57)	−21.06	−19.41 (−18.65)	−20.49	−18.79 (−18.05)

[a]Optimized with ADC(2)/def2-TZVPP. Excitation energies with ADC(2)/def2-TZVPPD. [b]Bond distances in pm. [c]Nonequilibrium corrected energies given in parentheses. [d]Experimental measurements yielded an emission band maximum of 3.41 eV.[75] [e]Experimental measurements yielded an emission band maximum of 4.03 eV.[75]

Downloaded from pubs.acs.org/jctce/article-pdf/22/13/6742/6590849/acs.jctc.6c00419.pdf by RUHR UNIVERSITAET BOCHUM user on 21 August 2026

https://doi.org/10.1021/acs.jctc.6c00419
J. Chem. Theory Comput. 2026, 22, 6742−6760

The experimentally measured emission band maxima in aqueous solution are 4.03 eV for phenol and 3.41 eV for phenolate.[75] For phenolate, COSMO predicts a solvent shift of 0.27−0.34 eV on the vertical emission energy, while EC-RISM gives somewhat larger shifts of 0.34−0.55 eV. Thus, the COSMO-CC2 result underestimates the experimental band maximum by 0.18−0.25 eV, whereas the EC-RISM result with PSE-3 including LR and nonequilibrium contributions is only blue-shifted by 0.03 eV. Independent of the solvent model, the calculated vertical emission energy for phenol is blue-shifted relative to experiment by approximately 0.5 eV, most likely for similar reasons as for the ground-state absorption.

The ΔpK_a^* values derived from the vertical transition energies agree less well with the values obtained from experimental emission band maxima from ref 75, although the influence of the various solvent effects is significantly smaller than for ground-state absorption. This indicates that remaining electronic structure errors and vibronic effects dominate the deviations from the experimental emission band maxima. Nevertheless, the results improve significantly from COSMO to EC-RISM.

Table 5 shows that single-point EC-RISM calculations on COSMO geometries already recover most of the solvent-model effect, but EC-RISM geometry optimization remains important when COSMO and EC-RISM differ strongly. For ΔpK_a^* from vertical absorption energies, the values improve from −14.45 with COSMO to −5.98 for EC-RISM on COSMO geometries and to −4.40 after full EC-RISM optimization, in almost quantitative agreement with the experimental value of −4.30. For the phenolate ground state, EC-RISM geometry optimization contributes approximately 0.1 eV, whereas the COSMO-to-EC-RISM energy change at the same structure is about five times larger.

Table 5. Comparison of Vertical Transition Energies of PhO^-[a]

structure	energy	excitation	emission
COSMO	COSMO	4.05	3.23
COSMO	EC-RISM/PSE-3	4.60	3.36
EC-RISM/PSE-3	EC-RISM/PSE-3	4.71	3.44

[a]Optimized with MP2/def2-TZVPP. Excitation and emission energies with ADC(2)/def2-TZVPPD including linear response and non-equilibrium corrections.

4.2.2. 3-Cyanophenol. The results for 3-cyanophenol and the 3-cyanophenolate anion are summarized in Tables 6 and 7.

The structural trends closely follow those observed for phenol. The largest solvent dependence occurs for the CO bond of the anion, which increases by up to 6.1 pm from vacuum to EC-RISM with PSE-3. For the neutral conformers, the CO bond changes less with solvation, whereas the OH bond length and the angle α increase from vacuum to COSMO to EC-RISM. In the excited state, the CO bond shortens for the neutral species but lengthens for the anion; in the latter case, the vacuum effect is partly canceled by solvation. The PSE order mainly affects hydrogen-bond-related coordinates.

Similar as for phenol and phenolate, also for 3-cyanophenol and the corresponding anion, there are clear differences between geometries obtained with COSMO and those obtained with EC-RISM. In this respect, both phenol and 3-cyanophenol differ from DMABN. In addition, the PSE order also visibly affects the geometry. The CO bond of the anion and the OH bond and the angle α of the neutral species are subject to the largest solvent effects. This illustrates that the solvent model has the strongest influence on bonds and angles directly involved in hydrogen bonding.

Table 6. Comparison of the Most Important Geometric Parameters and the Vertical Excitation Energies of 3-Cyano-PhOH/3-Cyano-PhO^- for the Ground State[a]

	vacuum	COSMO	PSE-2	PSE-3
3-Cyano-PhO^- Anion				
$d(C_1O)$[b]	126.3	128.5	132.1	132.4
$d(C_3C_7)$[b]	143.1	142.9	142.5	142.6
$d(C_7N)$[b]	117.6	117.4	117.1	117.1
$\Delta E(S_1)$[c]	3.32	3.61	4.19	4.23
$\Delta E(S_1)$ LR[c,d]		3.56 (3.52)	4.14 (4.11)	4.19 (4.16)
3-Cyano-PhOH (Conformer NC0)				
$d(C_1O)$[b]	136.1	136.0	135.6	135.6
$d(C_3C_7)$[b]	143.1	143.0	142.7	142.7
$d(C_7N)$[b]	117.3	117.2	117.0	117.0
$d(OH)$[b]	96.2	96.6	98.0	98.4
$\alpha(C_1OH)$ (deg)	109	109	111	111
$\Delta E(S_1)$[e]	4.67	4.62	4.63	4.62
$\Delta E(S_1)$ LR[d,e]		4.58 (4.61)	4.59 (4.58)	4.59 (4.58)
3-Cyano-PhOH (Conformer NC1)				
$d(C_1O)$[b]	136.1	136.0	135.6	135.5
$d(C_3C_7)$[b]	143.2	143.1	142.7	142.7
$d(C_7N)$[b]	117.3	117.2	117.0	117.0
$d(OH)$[b]	96.2	96.6	98.1	98.7
$\alpha(C_1OH)$ (deg)	109	109	110	110
$\Delta E(S_1)$[e]	4.66	4.61	4.62	4.61
$\Delta E(S_1)$ LR[d,e]		4.58 (4.60)	4.58 (4.57)	4.58 (4.56)
pK_a Change				
ΔpK_a^*	−22.75	−16.96	−7.34	−6.50
ΔpK_a^* LR[d]		−17.26 (−18.34)	−7.55 (−7.85)	−6.60 (−6.91)

[a]Geometry optimization with MP2/def2-TZVPP, excitation energies with ADC(2)/def2-TZVPPD. [b]Bond distances in pm. [c]Experimental measurements yielded an absorption band maximum of 3.79 eV.[77] [d]Nonequilibrium corrected energies given in parentheses. [e]Experimental measurements yielded an absorption band maximum of 4.23 eV.[77]

For the vertical excitation energies, the LR contribution is about −0.03 eV for the neutral conformers and up to −0.05 eV for the anion. The calculated excitation energies of the neutral conformers are all blue-shifted relative to the experiment value[77] of 4.23 eV. In contrast to EC-RISM, the absorption energy of the anion in vacuum and COSMO calculations is red-shifted relative to the experimental value[77] of 3.79 eV. Since the experimental band maximum are compared with vertical excitation energies here, the COSMO result contradicts the expected trend.

For the neutral conformers, excitation energies calculated with COSMO and EC-RISM differ only slightly, by 0.01 eV, while differences of 0.05 eV are observed between vacuum and solution. For the anion, however, differences of up to 0.42 eV are found between COSMO and EC-RISM and up to 0.71 eV between vacuum and solution.

Compared to the ΔpK_a^* value of −7.34 derived from experimental absorption energies, the value obtained from the EC-RISM results provides a significant improvement over COSMO.[31]

Downloaded from pubs.acs.org/jctce/article-pdf/22/13/6742/6590849/acs.jctc.6c00419.pdf by RUHR UNIVERSITAET BOCHUM user on 21 August 2026

https://doi.org/10.1021/acs.jctc.6c00419
J. Chem. Theory Comput. 2026, 22, 6742−6760

Table 7. Comparison of the Most Important Geometric Parameters and the Vertical Transition Energies of 3-Cyano-PhOH/3-Cyano-PhO$^-$ for the Excited State[a]

	vac	COSMO	COSMO-LR	PSE-2	PSE-2-LR	PSE-3	PSE-3-LR
				3-Cyano-PhO$^-$ Anion			
$d(C_1O)$[b]	138.4	138.1	137.5	137.6	136.8	137.6	136.8
$d(C_3C_7)$[b]	139.4	138.8	138.8	138.0	138.0	138.0	138.0
$d(C_7N)$[b]	119.2	119.5	119.5	119.4	119.4	119.4	119.4
$\Delta E(S_1)$[c,d]	2.17	2.19	2.20 (2.30)	2.21	2.24 (2.34)	2.22	2.25 (2.35)
				3-Cyano-PhOH (Conformer NC0)			
$d(C_1O)$[b]	134.5	133.8	133.6	133.2	132.9	133.2	132.9
$d(C_3C_7)$[b]	140.3	139.7	139.6	139.1	139.1	139.1	139.0
$d(C_7N)$[b]	118.2	118.6	118.6	118.5	118.6	118.6	118.6
$d(OH)$[b]	96.9	97.5	97.5	99.8	99.8	100.9	102.2
$\alpha(C_1OH)$ (deg)	109	110	110	112	112	113	114
$\Delta E(S_1)$[d,e]	4.27	4.09	4.04 (4.05)	4.02	3.95 (3.97)	3.99	3.92 (3.94)
				3-Cyano-PhOH (Conformer NC1)			
$d(C_1O)$[b]	134.6	133.8	133.6	133.2	133.0	133.0	132.7
$d(C_3C_7)$[b]	140.3	139.7	139.6	139.1	139.0	139.0	138.9
$d(C_7N)$[b]	118.2	118.6	118.6	118.6	118.6	118.6	118.7
$d(OH)$[b]	96.9	97.5	97.5	99.9	99.9	102.6	102.8
$\alpha(C_1OH)$ (deg)	108	110	110	112	112	112	112
$\Delta E(S_1)$[d,e]	4.26	4.09	4.03 (4.05)	4.00	3.94 (3.96)	3.94	3.89 (3.90)
				pK_a Change[d]			
ΔpK_a^*	−35.39	−32.10	−30.93 (−29.57)	−30.39	−28.73 (−27.38)	−29.55	−27.75 (−26.42)

[a]Optimized with ADC(2)/def2-TZVPP. Transition energies were computed with ADC(2)/def2-TZVPPD. [b]Bond distances in pm. [c]Experimental measurements yielded an emission band maximum of 3.06 eV.[75] [d]Nonequilibrium corrected energies given in parentheses. [e]Experimental measurements yielded an emission band maximum of 3.75 eV.[75]

For the neutral species, emission energies differ by 0.07−0.15 eV among the solvent models, while PSE-order and excitonic-coupling effects reach up to 0.07 eV. The nonequilibrium contribution is smaller, up to 0.02 eV. The experimentally measured emission energy of the anion is 3.06 eV, and that of the neutral species 3.75 eV.[75] The calculated emission energy of neutral 3-cyanophenol is blue-shifted relative to experiment by 0.17 eV for PSE-3 with LR effects. The emission energy of the anion is red-shifted by 0.71 eV for PSE-3 including LR and nonequilibrium contributions.

Since emission may occur before the excited-state minimum is reached, larger deviations between calculated and experimental values are possible. The ΔpK_a^* values derived from vertical transition energies agree less well with the value of −11.54 obtained from the experimental emission maxima than in the case of absorption. The differences between vacuum, COSMO, and EC-RISM are also significantly smaller.[75] Nevertheless, a systematic improvement is observed with the solvent model.

A comparison of different basis sets for 3-cyanophenol, shown in Table 8, indicates that def2-TZVP is sufficient for describing the ground state. However, def2-TZVPP is required for geometry optimization in the excited state. With the smaller basis set, the ring is not planar in the excited state, as indicated by the puckering amplitude.[78]

4.2.3. 7-Amino-4-methylcoumarin. The results for the ground-state structure of 7-amino-4-methylcoumarin (AMC), or coumarin 120, and its protonated cation, as well as the corresponding excitation energies, are summarized in Table 9. Table 10 summarizes the optimized excited-state geometries and emission energies.

For neutral AMC, solvent effects mainly affect the lactone and amino groups. In the ground state, the largest change is the shortening of the C_2O_1 bond by 2.7 pm from vacuum to EC-RISM, of which COSMO captures only about half. In the excited state, the lactone ring becomes more puckered, with amplitudes of 2 pm in vacuum, 6 pm with EC-RISM, and 23 pm with COSMO. Excitation also planarizes the amino group in solution, reducing its out-of-plane angle from 32° in vacuum to 0°, consistent with increased charge transfer into the aromatic system. For several lactone-ring bonds, the differences between COSMO and EC-RISM exceed 1 pm, with the C_2O_1 bond exhibiting a particularly pronounced solvent-model dependence.

PSE-order and LR effects on the structures are generally small. The largest PSE-order effect occurs for the OH bond of the protonated form, with changes of ∼1.5 pm in the ground state and ∼0.8 pm in the excited state.

For the protonated form, solvent effects are stronger in the ground state than in the excited state. In the ground state, the amino group changes from planar in vacuum to an out-of-plane angle of about 35° in solution. The largest bond-length changes are found for the CN bond (+1.9 pm) and the C_2═O bond (−1.3 pm), indicating reduced charge transfer from the

Table 8. Comparison of Geometric Parameters of 3-Cyanophenol in the Ground and Excited State for Different Basis sets[a]

	def-TZVP		def2-TZVPP	
	GS	ES	GS	ES
$d(C_1O)$[b]	136.2	133.7	135.6	133.2
$d(OH)$[b]	98.3	100.1	98.0	99.8
Q[c]	4.7	17.9	0.0	0.0

[a]Geometry optimization done with MP2 for the ground and with ADC(2) for the excited state. [b]Bond distances in pm. [c]Total puckering amplitude, indicating the magnitude of deviation from a planar ring.[78]

Downloaded from pubs.acs.org/jctce/article-pdf/22/13/6742/6590849/acs.jctc.6c00419.pdf by RUHR UNIVERSITAET BOCHUM user on 21 August 2026

https://doi.org/10.1021/acs.jctc.6c00419
J. Chem. Theory Comput. 2026, 22, 6742−6760

Table 9. Comparison of the Most Important Geometric Parameters and Vertical Excitation Energies of AMC for the Ground State[a]

	vac	COSMO	PSE-2	PSE-3
Coumarin 120 (Neutral)				
$d(C_3C_4)$[b]	135.5	135.8	135.7	135.8
$d(C_2C_3)$[b]	145.2	144.2	143.5	143.5
$d(C_2{=}O)$[b]	120.8	122.1	122.7	122.7
$d(C_2O_1)$[b]	138.7	137.3	136.1	136.0
$d(CN)$[b]	139.2	138.6	139.0	139.1
$d(NH)$[b]	100.7	100.9	101.3	101.4
$d(C_{10}O_1)$[b]	136.4	137.3	137.1	137.1
ϕ (deg)[c]	42	42	45	45
$\Delta E(S_1)$[d]	4.12	3.98	4.00	4.01
$\Delta E(S_1)$ LR[d,e]		3.90 (3.86)	3.92 (3.88)	3.93 (3.89)
Coumarin 120 (Protonated)				
$d(C_3C_4)$[b]	138.4	138.0	137.5	137.5
$d(C_2C_3)$[b]	138.6	139.0	139.2	139.4
$d(C_2{=}O)$[b]	131.0	130.7	129.9	129.7
$d(C_2O_1)$[b]	131.5	131.1	131.1	131.1
$d(CN)$[b]	134.8	135.9	136.5	136.7
$d(NH)$[b]	100.4	100.7	101.1	101.2
$d(C_{10}O_1)$[b]	137.9	137.7	137.5	137.4
$d(OH)$[b]	97.0	97.3	100.1	101.6
α(COH) (deg)	111	111	112	112
ϕ (deg)[c]	0	28	34	35
$\Delta E(S_1)$	3.11	3.23	3.33	3.36
$\Delta E(S_1)$ LR[e]		3.15 (3.11)	3.25 (3.20)	3.28 (3.23)
pK_a Change				
ΔpK_a^*	17.07	12.74	11.33	11.06
ΔpK_a^* LR[e]	17.07	12.69 (12.85)	11.28 (11.50)	10.95 (11.16)

[a]Optimized with MP2/def2-TZVPP. Excitation energies with ADC(2)/def2-TZVPPD. [b]Bond distances in pm. [c]Out-of-plane angle of the amino group. Here defined as angle between the plane containing N and the amino hydrogen atoms and the line connecting N with C_8. [d]Experimental measurements yielded an absorption band maximum of 3.62 eV.[79] [e]Nonequilibrium corrected energies given in parentheses.

amino to the carbonyl group in aqueous solution. COSMO captures only about half of this structural solvent effect. In the excited state, the amino and lactone groups remain planar, and the largest COSMO-EC-RISM difference is found for the OH bond with up to 2.6 pm.

For the neutral species, absorption energies calculated with COSMO and EC-RISM differ only marginally, by 0.03 eV. In contrast, for the cation, the directional interactions included in EC-RISM affect the absorption energy by up to 0.13 eV. Excitonic coupling lowers the results by up to 0.08 eV, and nonequilibrium corrections lower them further by 0.04 to 0.05 eV. Including these corrections, the computed solvent shifts of the absorption energies are between −0.23 and −0.26 eV for the neutral molecule and between 0.00 and +0.12 eV for the cation.

For the emission energies, excitonic coupling and nonequilibrium corrections have opposite signs and partially cancel, so that their combined effect is ≤0.03 eV for both the neutral and protonated forms. The computed solvent shift for the fluorescence energy of the neutral molecule is −0.56 eV for COSMO, whereas EC-RISM gives larger red shifts of −0.65 eV for PSE-2 and −0.68 eV for PSE-3. For the cation, the computed solvent shifts including LR and nonequilibrium corrections are smaller with values of 0.48 eV for COSMO and 0.47 eV for EC-RISM. Despite structural differences, the two solvent models give almost identical vertical emission energies for the cation.

For the neutral 7-amino-4-methylcoumarin in aqueous solution, the experimental absorption maximum is 3.62 eV and the emission maximum is 2.82 eV.[79] The computed vertical excitation energies of 3.86−3.98 eV obtained with COSMO-ADC(2) and EC-RISM-ADC(2) are blue-shifted by about 0.25 eV relative to experiment. Better agreement can not be expected for a comparison of vertical excitation energies with band maxima in aqueous solution. The computed vertical emission energies also agree well with experiment, 2.73 eV for COSMO and 2.61 and 2.64 eV for EC-RISM with, PSE-2 and PSE-3, respectively, corresponding to deviations between −0.09 and −0.21 eV.

5. CONCLUSION

We have developed an interface of TURBOMOLE to 3D-RISM and implemented the EC-RISM solvent model for ground-state energies and gradients at the HF, DFT, MP2, and CC2 level and for excitation energies and excited-state gradients with CC2 and ADC(2). While EC-RISM had already before been implemented for HF and DFT ground-state energies and gradients[12,52] as well as for MP2 energies[15] and TD-DFT excitation energies,[20] we implemented it here for the first time for ground- and excited-state gradients in combination with correlated wave function methods. The self-consistent PTED coupling scheme and the representation of the solute potential and the solvent charges on a common grid facilitated the implementation of nuclear gradients in a straightforward manner. Since EC-RISM does not distinguish between the nuclear and the electronic response of the solvent due the fixed-charge description of the solvent species, we combined it with the COSMO model to evaluate the LR (or excitonic coupling) contribution and nonequilibrium corrections to vertical electronic transition energies.

Applications to four test systems in aqueous solution—DMABN, phenol, 3-cyanophenol, and coumarin 120—demonstrate the capabilities of the implementation for modeling solvent effects on ground- and excited-state structures and electronic transition energies. The results show the influence of the additional description of directional interactions between solvent and solute, that are not accounted for by apparent surface models like COSMO but included with EC-RISM, on molecular structures in ground and excited states and on absorption and emission energies. When comparing the results obtained with the COSMO and EC-RISM solvent models, it becomes apparent that comparable results are obtained for systems that do not form strong hydrogen bonds with the solvent. However, if strong interactions occur between solvent and solute, as is the case for phenolate anions and the protonated coumarin 120 in water, the solvent model has a strong influence. While COSMO dramatically overestimates ΔpK_a^* for phenols, EC-RISM achieves remarkable agreement between experiment and calculation. This effect already occurs when computing the energies with EC-RISM using structures optimized with COSMO. However, when the geometry optimizations are done with EC-RISM the results for the transition energies and ΔpK_a^* improve further. For bond lengths sensitive to hydrogen bonding between solute and solvent, COSMO often captures only about half of the effects found with EC-RISM.

Downloaded from pubs.acs.org/jctce/article-pdf/22/13/6742/6590384/acs.jctc.6c00419.pdf by RUHR UNIVERSITAET BOCHUM user on 21 August 2026

https://doi.org/10.1021/acs.jctc.6c00419
J. Chem. Theory Comput. 2026, 22, 6742−6760

Table 10. Comparison of the Most Important Geometric Parameters and Vertical Transition Energies of 7-Amino-4-methylcoumarin (Coumarin 120) for the Excited State[a]

	vac	COSMO	COSMO-LR	PSE-2	PSE-2-LR	PSE-3	PSE-3-LR
			Coumarin 120 (Neutral)[g]				
$d(C_3C_4)$[b]	144.9	142.0	142.3	139.8	139.8	139.7	139.7
$d(C_2C_3)$[b]	138.5	140.1	140.0	139.6	139.7	139.6	139.7
$d(C_2{=}O)$[b]	123.3	124.8	124.9	127.2	127.0	127.5	127.2
$d(C_2O_1)$[b]	147.1	142.7	142.6	140.0	139.7	139.8	139.5
$d(CN)$[b]	137.6	134.6	134.6	134.5	134.5	134.5	134.5
$d(NH)$[b]	100.7	101.0	101.0	101.7	101.7	101.7	101.7
$d(C_{10}O_1)$[b]	133.2	136.5	136.6	136.6	136.9	136.6	136.9
ϕ (deg)[c]	32	0	0	0	0	0	0
Q[d]	1.5	22.6	19.2	3.3	5.8	3.7	5.6
$\Delta E(S_1)$[e,f]	3.29	2.70	2.69 (2.73)	2.64	2.59 (2.64)	2.61	2.56 (2.61)
			Coumarin 120 (Protonated)				
$d(C_3C_4)$[b]	139.1	138.1	138.4	137.9	137.9	137.9	137.9
$d(C_2C_3)$[b]	138.5	138.8	138.7	138.7	138.7	138.8	138.9
$d(C_2{=}O)$[b]	133.0	133.8	133.6	133.3	133.1	133.2	133.0
$d(C_2O_1)$[b]	136.2	135.7	135.5	135.5	135.3	135.6	135.3
$d(CN)$[b]	134.8	134.8	134.8	134.6	134.6	134.6	134.6
$d(NH)$[b]	101.0	101.3	101.3	101.9	101.9	101.9	101.9
$d(C_{10}O_1)$[b]	137.2	137.1	137.4	136.9	137.2	136.9	137.2
$d(OH)$[b]	96.7	97.0	97.0	98.8	98.9	99.6	99.6
α(COH) (deg)	110	110	110	111	111	111	111
$\Delta E(S_1)$[e]	2.67	2.16	2.14 (2.19)	2.18	2.14 (2.20)	2.18	2.14 (2.20)
			pK_a Change[e]				
ΔpK_a^*		9.17	9.41 (9.19)	7.78	7.46 (7.40)	7.25	7.07 (7.02)

[a]Optimized with ADC(2)/def2-TZVPP. Transition energies with ADC(2)/def2-TZVPPD. [b]Bond distances in pm. [c]Out-of-plane angle of the amino group. Here defined as angle between the plane containing N and the amino hydrogen atoms and the line connecting N with C_8. [d]Total puckering amplitude, indicating the magnitude of deviation from a flat ring.[78] [e]Nonequilibrium corrected energies given in parentheses. [f]Experimental measurements yielded an emission band maximum of 2.82 eV.[79] [g]Norm of remaining gradient in vacuum: 1×10^{-2} a.u.

For the absorption energies obtained with EC-RISM-ADC(2) or EC-RISM-CC2, the remaining source of error is probably mostly related to the comparison of computed vertical transition energies with experimental band maxima. Because of reduced bond strengths after excitation of an electron into an antibonding orbital, the structures in the excited states are more sensitive to the choice of solvent model and accurate emission energies require in some cases higher order electronic structure methods.

Finally, it can be said that although EC-RISM is computationally more demanding than apparent surface charge models like COSMO, the difference in computational costs is small (about a factor of 1.5−2 for 3-cyanophenol, see Section S5 of the Supporting Information) compared to the overall costs for self-consistent PTED calculations with correlated wave function methods and considering the substantial improvement of the results seen in critical cases.

■ ASSOCIATED CONTENT

Data Availability Statement

Data for this article, including structures, input files, and output files are available at RESOLVdata[80] at https://doi.org/10.17877/RESOLV-2026-MKZU5UDM.

Supporting Information

The Supporting Information is available free of charge at https://pubs.acs.org/doi/10.1021/acs.jctc.6c00419.

The Supporting Information contains additional details on the gradient contributions from translation of the grid, the handling of contributions violating rotational invariance, and a derivation of the nonequilibrium corrections. Furthermore, it reports additional results for the validation of the gradient implementation, the effect of the long-range correction for the electrostatic potential, convergence with grid parameters, a comparison of geometry optimizations with and without diffuse basis functions, a comparison of timings for COSMO and EC-RISM, and the dominant NTOs for the transitions in the four example molecules (PDF)

■ AUTHOR INFORMATION

Corresponding Author

Julia Haberhauer − *Lehrstuhl für Theoretische Chemie, Ruhr-Universität Bochum, 44780 Bochum, Germany;* orcid.org/0000-0002-0100-1959; Email: julia.haberhauer@ruhr-uni-bochum.de

Authors

Patrick Kibies − *Fakultät für Chemie und Chemische Biologie, Technische Universität Dortmund, 44227 Dortmund, Germany*

Stefan M. Kast − *Fakultät für Chemie und Chemische Biologie, Technische Universität Dortmund, 44227 Dortmund, Germany;* orcid.org/0000-0001-7346-7064

Christof Hättig − *Lehrstuhl für Theoretische Chemie, Ruhr-Universität Bochum, 44780 Bochum, Germany;* orcid.org/0000-0002-5752-2710

Complete contact information is available at: https://pubs.acs.org/10.1021/acs.jctc.6c00419

Downloaded from pubs.acs.org/jctce/article-pdf/22/13/6742/6590849/acs.jctc.6c00419.pdf by RUHR UNIVERSITAET BOCHUM user on 21 August 2026

Notes

The authors declare no competing financial interest.

■ ACKNOWLEDGMENTS

Funded by the Deutsche Forschungsgemeinschaft (DFG, German Research Foundation) under Germany's Excellence Strategy-EXC 2033-390677874-RESOLV.

■ REFERENCES

(1) Tomasi, J.; Persico, M. Molecular Interactions in Solution: An Overview of Methods Based on Continuous Distributions of the Solvent. *Chem. Rev.* **1994**, *94*, 2027−2094.
(2) Mennucci, B. Polarizable continuum model. *Wiley Interdiscip. Rev.: Comput. Mol. Sci.* **2012**, *2*, 386.
(3) Klamt, A.; Schüürmann, G. COSMO: a new approach to dielectric screening in solvents with explicit expressions for the screening energy and its gradient. *J. Chem. Soc., Perkin Trans. 2* **1993**, 799.
(4) Kloss, T.; Heil, J.; Kast, S. M. Quantum Chemistry in Solution by Combining 3D Integral Equation Theory with a Cluster Embedding Approach. *J. Phys. Chem. B* **2008**, *112*, 4337−4343.
(5) Tielker, N.; Eberlein, L.; Güssregen, S.; Kast, S. M. The SAMPL6 challenge on predicting aqueous pKa values from EC-RISM theory. *J. Comput.-Aided Mol. Des.* **2018**, *32*, 1151−1163.
(6) Ikeguchi, M.; Doi, J. Direct numerical solution of the Ornstein−Zernike integral equation and spatial distribution of water around hydrophobic molecules. *J. Chem. Phys.* **1995**, *103*, 5011−5017.
(7) Beglov, D.; Roux, B. An Integral Equation To Describe the Solvation of Polar Molecules in Liquid Water. *J. Phys. Chem. B* **1997**, *101*, 7821−7826.
(8) Kovalenko, A.; Hirata, F. Three-dimensional density profiles of water in contact with a solute of arbitrary shape: a RISM approach. *Chem. Phys. Lett.* **1998**, *290*, 237−244.
(9) Kovalenko, A.; Gusarov, S. Multiscale methods framework: self-consistent coupling of molecular theory of solvation with quantum chemistry, molecular simulations, and dissipative particle dynamics. *Phys. Chem. Chem. Phys.* **2018**, *20*, 2947.
(10) Yoshida, N.; Yamaguchi, T.; Nakano, H. Implementation of solvent polarization in three-dimensional reference interaction-site model self-consistent field theory. *Chem. Phys. Lett.* **2022**, *797*, 139579.
(11) Yokogawa, D. New Generation of the Reference Interaction Site Model Self-Consistent Field Method: Introduction of Constrained Spatial Electron Density Distribution (cSED). *Bull. Chem. Soc. Jpn.* **2018**, *91*, 1540−1545.
(12) Hölzl, C.; Kibies, P.; Imoto, S.; Frach, R.; Suladze, S.; Winter, R.; Marx, D.; Horinek, D.; Kast, S. M. Design principles for high−pressure force fields: Aqueous TMAO solutions from ambient to kilobar pressures. *J. Chem. Phys.* **2016**, *144*, 144104.
(13) Sharma, B.; Tran, V. A.; Pongratz, T.; Galazzo, L.; Zhurko, I.; Bordignon, E.; Kast, S. M.; Neese, F.; Marx, D. A Joint Venture of Ab Initio Molecular Dynamics, Coupled Cluster Electronic Structure Methods, and Liquid-State Theory to Compute Accurate Isotropic Hyperfine Constants of Nitroxide Probes in Water. *J. Chem. Theory Comput.* **2021**, *17*, 6366−6386.
(14) Tran, V. A.; Teucher, M.; Galazzo, L.; Sharma, B.; Pongratz, T.; Kast, S. M.; Marx, D.; Bordignon, E.; Schnegg, A.; Neese, F. Dissecting the Molecular Origin of g-Tensor Heterogeneity and Strain in Nitroxide Radicals in Water: Electron Paramagnetic Resonance Experiment versus Theory. *J. Phys. Chem. A* **2023**, *127*, 6447−6466.
(15) Ganyecz, Á.; Kállay, M. Implementation and Optimization of the Embedded Cluster Reference Interaction Site Model with Atomic Charges. *J. Phys. Chem. A* **2022**, *126*, 2417−2429.
(16) Maste, S.; Sharma, B.; Pongratz, T.; Grabe, B.; Hiller, W.; Erlach, M. B.; Kremer, W.; Kalbitzer, H. R.; Marx, D.; Kast, S. M. The accuracy limit of chemical shift predictions for species in aqueous solution. *Phys. Chem. Chem. Phys.* **2024**, *26*, 6386−6395.
(17) Pongratz, T.; et al. Pressure-Dependent Electronic Structure Calculations Using Integral Equation-Based Solvation Models. *Biophys. Chem.* **2020**, *257*, 106258.
(18) Wada, T.; Nakano, H.; Sato, H. Solvatochromic Shift of Brooker's Merocyanine: Hartree−Fock Exchange in Time Dependent Density Functional Calculation and Hydrogen Bonding Effect. *J. Chem. Theory Comput.* **2014**, *10*, 4535−4547.
(19) Tanaka, Y.; Yoshida, N.; Nakano, H. Solvent effect on excited states of merocyanines: A theoretical study using the RISM−SCF method. *Chem. Phys. Lett.* **2013**, *583*, 69−73.
(20) Reimann, M.; Kaupp, M. Evaluation of an Efficient 3D-RISM-SCF Implementation as a Tool for Computational Spectroscopy in Solution. *J. Phys. Chem. A* **2020**, *124*, 7439−7452.
(21) Imamura, K.; Yokogawa, D.; Sato, H. Recent developments and applications of reference interaction site model self-consistent field with constrained spatial electron density (RISM-SCF-cSED): A hybrid model of quantum chemistry and integral equation theory of molecular liquids. *J. Chem. Phys.* **2024**, *160*, 050901.
(22) Tapia, O. On the theory of solvent-effect representation: Part I. A generalized self-consistent reaction field theory. *J. Mol. Struct.* **1991**, *226*, 59−72.
(23) del Valle, F.; Tomasi, J. Electron correlation and solvation effects. I. Basic formulation and preliminary attempt to include the electron correlation in the quantum mechanical polarizable continuum model so as to study solvation phenomena. *Chem. Phys.* **1991**, *150*, 139.
(24) Cammi, R.; Corni, S.; Mennucci, B.; Tomasi, J. Electronic excitation energies of molecules in solution: State specific and linear response methods for nonequilibrium continuum solvation models. *J. Chem. Phys.* **2005**, *122*, 104513.
(25) Lunkenheimer, B.; Köhn, A. Solvent Effects on Electronically Excited States Using the Conductor-Like Screening Model and the Second-Order Correlated Method ADC(2). *J. Chem. Theory Comput.* **2013**, *9*, 977−994.
(26) Caricato, M.; Mennucci, B.; Tomasi, J.; Ingrosso, F.; Cammi, R.; Corni, S.; Scalmani, G. Formation and relaxation of excited states in solution: A new time dependent polarizable continuum model based on time dependent density functional theory. *J. Chem. Phys.* **2006**, *124*, 124520.
(27) Improta, R.; Barone, V.; Scalmani, G.; Frisch, M. J. A state-specific polarizable continuum model time dependent density functional theory method for excited state calculations in solution. *J. Chem. Phys.* **2006**, *125*, 054103.
(28) Marenich, A. V.; Cramer, C. J.; Truhlar, D. G.; Guido, C. A.; Mennucci, B.; Scalmani, G.; Frisch, M. J. Practical computation of electronic excitation in solution: vertical excitation model. *Chem. Sci.* **2011**, *2*, 2143−2161.
(29) Christiansen, O.; Koch, H.; Jørgensen, P. The second-order approximate coupled cluster singles and doubles model CC2. *Chem. Phys. Lett.* **1995**, *243*, 409−418.
(30) Hättig, C.; Pausch, A. Gradients of Ground and Excited States for CC2 and ADC(2) in Polarizable Continuum and Atomistic Embeddings within a Generalized PTED Coupling Scheme. *J. Phys. Chem. A* **2025**, *129*, 6155−6169.
(31) Tiska, Ö. F. C.; Sülzner, N.; Haberhauer, J.; Kibies, P.; Kast, S. M.; Hättig, C. Comparison of the solvation models COSMO and EC-RISM for the prediction of photoacidity in aqueous solution. *Phys. Chem. Chem. Phys.* **2025**, *27*, 17930.
(32) Sermoud, V. d. M.; de Freitas Gonçalves, A.; Barreto, A. G.; Franco, L. F. M.; Tavares, F. W.; Castier, M. Classical density functional theory of confined fluids: From getting started to modern applications. *Fluid Phase Equilib.* **2024**, *586*, 114177.
(33) Hansen, J.-P.; McDonald, I. R. *Theory of Simple Liquids*, 4th ed.; Academic Press, 2013.
(34) Ornstein, L. S.; Zernike, F. Accidental deviations of density and opalescence at the critical point of a single substance. *Proc. Akad. Sci.* **1914**, *17*, 793−806.

Downloaded from pubs.acs.org/jctce/article-pdf/22/13/6742/6590849/acs.jctc.6c00419.pdf by RUHR UNIVERSITAET BOCHUM user on 21 August 2026

(35) Kast, S. M.; Kloss, T. Closed-form expressions of the chemical potential for integral equation closures with certain bridge functions. *J. Chem. Phys.* **2008**, *129*, 236101.
(36) Kovalenko, A.; Hirata, F. Potentials of mean force of simple ions in ambient aqueous solution. I. Three-dimensional reference interaction site model approach. *J. Chem. Phys.* **2000**, *112*, 10391.
(37) Morita, T.; Hiroike, K. A New Approach to the Theory of Classical Fluids. III: General Treatment of Classical Systems. *Prog. Theor. Phys.* **1961**, *25*, 537−578.
(38) Kovalenko, A.; Hirata, F. Self-consistent description of a metal−water interface by the Kohn−Sham density functional theory and the three-dimensional reference interaction site model. *J. Chem. Phys.* **1999**, *110*, 10095.
(39) Singer, S. J.; Chandler, D. Free energy functions in the extended RISM approximation. *Mol. Phys.* **1985**, *55*, 621−625.
(40) Heil, J.; Kast, S. M. 3D RISM theory with fast reciprocal-space electrostatics. *J. Chem. Phys.* **2015**, *142*, 114107.
(41) Hoffgaard, F.; Heil, J.; Kast, S. M. Three-Dimensional RISM Integral Equation Theory for Polarizable Solute Models. *J. Chem. Theory Comput.* **2013**, *9*, 4718−4726.
(42) Kibies, P. J. Integral equation-based calculations of the electronic structure of small molecules under high pressure. Doctoral Thesis, Technische Universität Dortmund, 2019.
(43) Helgaker, T.; Jørgensen, P.; Olsen, J. *Molecular Electronic-Structure Theory*; John Wiley and Sons: New York, 2000.
(44) Hättig, C. Geometry optimizations with the coupled-cluster model CC2 using the resolution-of-the-identity approximation. *J. Chem. Phys.* **2003**, *118*, 7751.
(45) Köhn, A.; Hättig, C. Analytic gradients for excited states in the coupled-cluster model CC2 employing the resolution-of-the-identity approximation. *J. Chem. Phys.* **2003**, *119*, 5021−5036.
(46) Schirmer, J. Beyond the random-phase approximation: A new approximation scheme for the polarization propagator. *Phys. Rev. A: At., Mol., Opt. Phys.* **1982**, *26*, 2395.
(47) Trofimov, A. B.; Schirmer, J. An efficient polarization propagator approach to valence electron excitation spectra. *J. Phys. B: At. Mol. Opt. Phys.* **1995**, *28*, 2299.
(48) Hättig, C. Structure optimizations for excited states with correlated second-order methods: CC2, CIS(D∞), and ADC(2). *Adv. Quantum Chem.* **2005**, *50*, 37−60.
(49) *TURBOMOLE V7.9 2024, a Development of University of Karlsruhe and Forschungszentrum Karlsruhe GmbH, 1989−2007*; TURBOMOLE GmbH, 2007. Available from https://www.turbomole.org.
(50) Franzke, Y. J.; et al. TURBOMOLE: Today and Tomorrow. *J. Chem. Theory Comput.* **2023**, *19*, 6859−6890.
(51) Hättig, C.; Weigend, F. CC2 excitation energy calculations on large molecules using the resolution of the identity approximation. *J. Chem. Phys.* **2000**, *113*, 5154.
(52) Gusarov, S.; Ziegler, T.; Kovalenko, A. Self-Consistent Combination of the Three-Dimensional RISM Theory of Molecular Solvation with Analytical Gradients and the Amsterdam Density Functional Package. *J. Phys. Chem. A* **2006**, *110*, 6083−6090.
(53) Heil, J. Effiziente Fluidphasentheorie für Protonierungsprozesse in komplexen Systemen. Doctoral Thesis, Technische Universität Dortmund, 2016.
(54) Corni, S.; Cammi, R.; Mennucci, B.; Tomasi, J. Electronic excitation energies of molecules in solution within continuum solvation models: Investigating the discrepancy between state-specific and linear-response methods. *J. Chem. Phys.* **2005**, *123*, 134512.
(55) Linder, B.; Lee, K.; Malinowski, P.; Tanner, A. On the relation between charge-density susceptibility, scattering functions, and Van Der Waals forces. *Chem. Phys.* **1980**, *52*, 353−361.
(56) Weigend, F.; Ahlrichs, R. Balanced basis sets of split valence, triple zeta valence and quadruple zeta valence quality for H to Rn: Design and assessment of accuracy. *Phys. Chem. Chem. Phys.* **2005**, *7*, 3297−3305.
(57) Rappoport, D.; Furche, F. Property-optimized Gaussian basis sets for molecular response calculations. *J. Chem. Phys.* **2010**, *133*, 134105.
(58) Häser, M.; Ahlrichs, R. Improvements on the direct SCF method. *J. Comput. Chem.* **1989**, *10*, 104−111.
(59) Hättig, C.; Hellweg, A.; Köhn, A. Distributed memory parallel implementation of energies and gradients for second-order Møller−Plesset perturbation theory with the resolution-of-the-identity approximation. *Phys. Chem. Chem. Phys.* **2006**, *8*, 1159.
(60) Hättig, C.; Köhn, A. Transition moments and excited-state first-order properties in the coupled-cluster model CC2 using the resolution-of-the-identity approximation. *J. Chem. Phys.* **2002**, *117*, 6939.
(61) Weigend, F.; Häser, M.; Patzelt, H.; Ahlrichs, R. RI-MP2: optimized auxiliary basis sets and demonstration of efficiency. *Chem. Phys. Lett.* **1998**, *294*, 143−152.
(62) Hellweg, A.; Rappoport, D. Development of new auxiliary basis functions of the Karlsruhe segmented contracted basis sets including diffuse basis functions (def2-SVPD, def2-TZVPPD, and def2-QVPPD) for RI-MP2 and RI-CC calculations. *Phys. Chem. Chem. Phys.* **2015**, *17*, 1010.
(63) Pausch, A. Consistent Analytical Second Derivatives of the Kohn−Sham DFT Energy in the Framework of the Conductor-Like Screening Model through Gaussian Charge Distributions. *J. Chem. Theory Comput.* **2024**, *20*, 3169−3183.
(64) Case, D. A.; et al. *Amber 2022 Reference Manual*; University of California: San Francisco, 2022.
(65) Singh, U. C.; Kollman, P. A. An approach to computing electrostatic charges for molecules. *J. Comput. Chem.* **1984**, *5*, 129−145.
(66) Besler, B. H.; Merz, Jr. K. M.; Kollman, P. A. Atomic charges derived from semiempirical methods. *J. Comput. Chem.* **1990**, *11*, 431−439.
(67) Kuznetsova, N. A.; Kaliya, O. L. The photochemistry of Coumarins. *Russ. Chem. Rev.* **1992**, *61*, 683−696.
(68) Gómez, S.; Soysal, E. N.; Worth, G. A. Micro-Solvated DMABN: Excited State Quantum Dynamics and Dual Fluorescence Spectra. *Molecules* **2021**, *26*, 7247.
(69) Rettig, W. Charge Separation in Excited States of Decoupled Systems—TICT Compounds and Implications Regarding the Development of New Laser Dyes and the Primary Process of Vision and Photosynthesis. *Angew. Chem., Int. Ed. Engl.* **1986**, *25*, 971−988.
(70) Grabowski, Z. R.; Rotkiewicz, K.; Rettig, W. Structural Changes Accompanying Intramolecular Electron Transfer: Focus on Twisted Intramolecular Charge-Transfer States and Structures. *Chem. Rev.* **2003**, *103*, 3899−4032.
(71) Köhn, A.; Hättig, C. On the Nature of the Low-Lying Singlet States of 4-(Dimethyl-amino)benzonitrile. *J. Am. Chem. Soc.* **2004**, *126*, 7399−7410.
(72) Bai, S.; Mansour, R.; Stojanović, L.; Toldo, J. M.; Barbatti, M. On the origin of the shift between vertical excitation and band maximum in molecular photoabsorption. *J. Mol. Model.* **2020**, *26*, 107.
(73) Sülzner, N.; Jung, G.; Nuernberger, P. A dual experimental−theoretical perspective on ESPT photoacids and their challenges ahead. *Chem. Sci.* **2025**, *16*, 1560−1596, DOI: 10.1039/D4SC07148D.
(74) Wehry, E. L.; Rogers, L. B. Application of Linear Free Energy Relations to Electronically Excited States of Monosubstituted Phenols. *J. Am. Chem. Soc.* **1965**, *87*, 4234−4238.
(75) Joung, J. F.; Jeong, M.; Park, S. Reliable experimental method for determination of photoacidity revealed by quantum chemical calculations. *Phys. Chem. Chem. Phys.* **2022**, *24*, 21714.
(76) Tsuru, S.; Sharma, B.; Hättig, C.; Marx, D. Nuclear Quantum Effects Have a Significant Impact on UV/Vis Absorption Spectra of Chromophores in Water. *Angew. Chem.* **2024**, *137*, No. e202416058.
(77) Schulman, S. G.; Vincent, W. R.; Underberg, W. J. M. Acidity of cyanophenols in the S1 and T1 states. The influence of substituent orientation. *J. Phys. Chem.* **1981**, *85*, 4068−4071.

Downloaded from pubs.acs.org/jctce/article-pdf/22/13/6742/6590849/acs.jctc.6c00419.pdf by RUHR UNIVERSITAET BOCHUM user on 21 August 2026

(78) Cremer, D.; Pople, J. A. General definition of ring puckering coordinates. *J. Am. Chem. Soc.* **1975**, *97*, 1354−1358.
(79) Bozkurt, E.; Onganer, Y. Photophysical features of coumarin 120 in reverse micelles. *J. Mol. Struct.* **2018**, *1173*, 490−497.
(80) Haberhauer, J.; Hättig, C. Replication Data for: "Implementation of EC-RISM for ADC(2) and CC2 to Include Solvent Granularity Effects in Excited-State Energies and Gradients", TUDOdata. **2026**, DOI: 10.17877/RESOLV-2026-MKZU5UDM (accessed May 13, 2026).

Downloaded from pubs.acs.org/jctcce/article-pdf/22/13/6742/6590384/acs.jctc.6c00419.pdf by RUHR UNIVERSITAET BOCHUM user on 21 August 2026

https://doi.org/10.1021/acs.jctc.6c00419
J. Chem. Theory Comput. 2026, 22, 6742−6760